LABORATORI NAZIONALI DI FRASCATI
SIS – Pubblicazioni

LNF-95/053 (P)
28 Settembre 1995

Total Hadronic Photoabsorption Cross Section on Nuclei in the Nucleon Resonance Region

N. Bianchi, V. Muccifora, E. De Sanctis, A. Fantoni, P. Levi Sandri, E. Polli, A.R. Reolon, P. Rossi

Istituto Nazionale di Fisica Nucleare - Laboratori Nazionali di Frascati

C.P. 13, I-00044, Frascati, Italy

M. Anghinolfi, P. Corvisiero, M. Ripani, M. Sanzone, M. Taiuti, A. Zucchiatti

Istituto Nazionale di Fisica Nucleare and Dipartimento di Fisica dell'Universitá

via Dodecaneso 33, I-16146 Genova, Italy

Abstract

The total photoabsorption cross section for ^{7}Li, C, Al, Cu, Sn, Pb has been measured in the energy range 300 ÷ 1200 MeV at Frascati with the Jet-Target tagged photon beam. A 4π NaI crystal detector and a lead-glass shower counter were used respectively to measure hadronic events and to reject the electromagnetic background. Data above 600 MeV clearly indicate a spreading out of higher nucleon resonance peaks in nuclei and a reduction of the absolute value of the cross section per nucleon respect to the free nucleon case. This large broadening of higher nucleon resonances suggests a strong influence of the nuclear medium in their propagation and interaction mechanisms, while the systematic reduction of the measured cross sections migth be due to a damping of the resonance excitation strength and to the onset of shadowing effect around 1 GeV. Moreover our systematic study indicates that also the Δ-resonance excitation parameters are not the same for all the nuclei, being its mass and width increasing with the nuclear density.

PACS.: 25.20.Gf

Submitted to Physical Review C

1. INTRODUCTION

The total photonuclear absorption cross section has been measured over wide mass number and photon energy ranges, yielding information on the influence of the nuclear medium on the intrinsic properties of nucleons in nuclei, as well as on the hadronic nature of the photon.[1]

Between 140 and 500 MeV, the total cross section per nucleon clearly exhibits the existence of the Δ in nuclei. This is not a trivial statement considering the composite structures of nucleon and Δ at the level of quarks and gluons: in general when such extended systems may overlap, their excitation spectra change as compared to the ones for isolated objects. Previous

data for various nuclei show that the resonance shape and strength are nearly universal within the systematic errors of different experiments (which were typically about $8 \div 10\%$), thus indicating an incoherent volume-photoabsorption mechanism. The average response of bound nucleons differs from that for the free nucleon, mainly because of Fermi motion, Pauli blocking and the propagation and interaction of the Δ in the nucleus, and has been generally treated in the framework of Δ-hole models[2]: however the total strength of the interaction is conserved. Moreover it is worth mentioning that none of the experiments was able to perform a systematic study of the process being each of them able to provide reliable data only over a limited range of mass number. Then, unlike the case of pion-absorption experiments,[3] no accurate experimental information was available on the possible influence of nuclear medium parameters like the size of the nucleus or the nuclear density on the first nucleon resonance excitation in the photon absorption mechanism.

Up to few years ago, much less information was available for the higher mass nucleon resonance photo-excitation in nuclei: sparse data were collected at Yerevan with large acceptance over the actual photon energy and with fluctuations well above the experimental errors.[4,5] Recently, the total nuclear photoabsorption cross section measurements carried out at Frascati with $200 \div 1200$ MeV tagged photons on ^{238}U,[6] Be and C[7,8] have revealed that in these nuclei there is no evidence of the excitation

of the $D_{13}(1520)$ and $F_{15}(1680)$ resonances clearly seen in the photoabsorption on hydrogen[9] and deuteron[10] and that above 600 MeV there is a damping of the absolute value of the cross section per nucleon with respect to what obtained from the deuteron data. On the contrary, the Δ resonance peak is only slightly distorted in nuclei in general agreement with the previous data available in the literature.[1] This experimental finding has been confirmed by the contemporary data on the photofission cross section for ^{238}U[11] and ^{235}U[12] obtained at Mainz up to 800 MeV.

This paper reports upon the complete analysis of the photoabsorption data obtained at Frascati on ^{7}Li, C, Al, Cu, Sn, Pb, using a tagged photon beam and the photohadronic method. In previous papers we published the preliminary and low statistic data obtained on C and CD_2[8] and the average nuclear behavior[13] of the total photoabsorption cross section.

2. THEORY

2.1. Δ resonance region

The dominant feature of photon interaction above the π-threshold ($140 < k < 500$ MeV, being k the energy of the photon) is the Δ-resonance excitation. Consequently photon-induced nuclear reactions in this energy region depend directly upon the dynamics of Δ-propagation through the nucleus. Pion-absorption and -scattering experiments suggested that this mechanism can be treated in the framework of a Δ-hole model in which the Δ is generated as a quasi-particle, propagates in the nucleus and interacts with nucleons through an empirical Δ-spreading complex nuclear potential composed by central and spin-orbit terms. The former term is proportional to the nuclear density and its real part is responsible for the mass shift of the Δ, while its imaginary part is responsible for the broadening of its width. The parameters of this complex potential are generally derived from the pion- nucleus elastic scattering amplitude and have been successfully applied also in the photon absorption and Compton scattering processes.[2] In contrast to the pion, the photon penetrates freely into the nuclear volume: this eliminates the strong shadowing due to multiple scattering of pions, so that the cross-section is expected to be roughly proportional to the mass number A.

Recently Carrasco and Oset[15] developed a microscopical model with a systematic many-body expansion in the number of Δ-hole excitations and with the inclusion of Pauli blocking, Fermi motion and non-resonant absorption channels: Fig.1 shows the result of their calculation for free nucleon, carbon and lead. As it is seen the damping and the shift of the peak and the increasing of the width are more evident for the heavier nucleus.

2.2. N^* resonance region

The new Frascati and Mainz photoabsorption data on nuclei above the Δ region ($k > 500$ MeV) have triggered different theoretical attempts to describe the higher nucleon resonance N^* behavior and to justify why the elementary photo-nucleon ab-

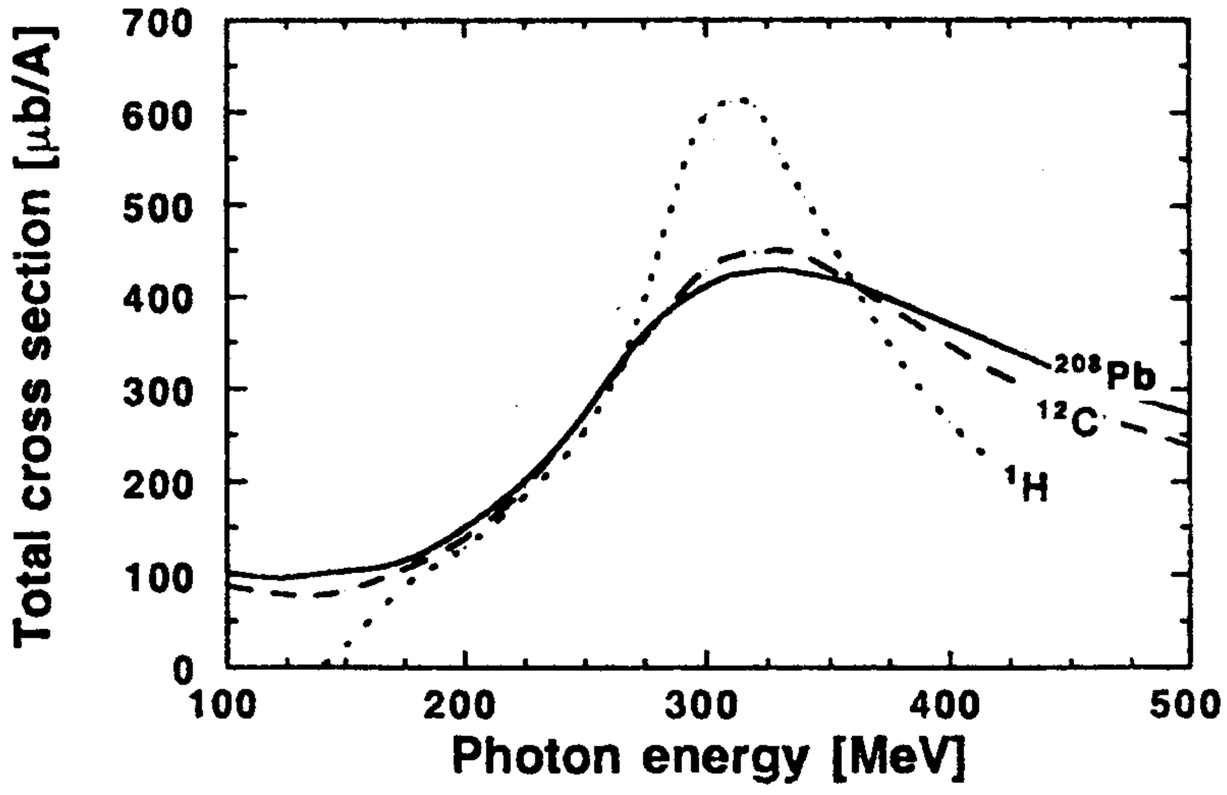

Fig. 1. Microscopical calculation for σ_A/A in the framework of a Δ-hole model: dashed line is the result for ^{12}C, continuos line for ^{208}Pb, while dotted line for the impulse approximation.[15]

sorption process is so widely modified inside the nuclei. Due to the large number of absorption channels and to the different dynamics and decay channels of N^* resonances, only simplified and very schematic models have been developed.

Kondratyuk *et al.*[16] tried to reproduce the experimental photofission cross section on ^{238}U[6] using a simple phenomenological model which allows the produced resonance to propagate inside the nucleus until it interacts with the surrounding nucleons. Due to such collisions, the mass and the width of the resonance increase in the nuclear matter. In order to reproduce the experimental data it was found necessary to use a higher collision cross section for the N^* resonances in the nuclei, producing a larger broadening of the D_{13} and F_{15} resonances with respect to the Δ. Alberico *et al.*[17] found similar results by employing a simple resonance-hole model and assuming that the nuclear medium strongly increases the width of all resonances above the Δ. In both the above approaches the strength of excitation of Δ and N^* resonances is conserved but spread out over a wide energy range. Fig. 2 shows how well these two

models reproduce our previous photofission cross section data on ^{238}U, which can be assumed to be almost equal to the total cross section.

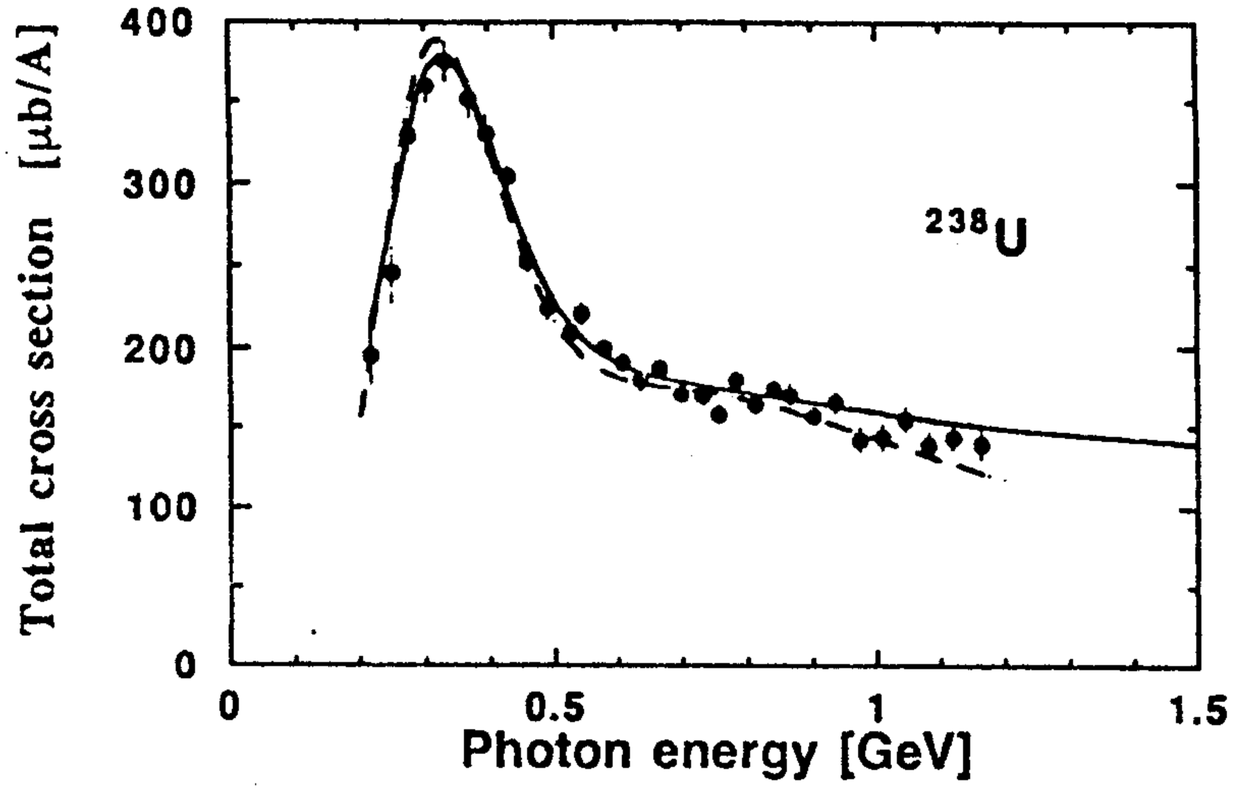

Fig. 2. Phenomenological fits to Frascati photofission data for ^{238}U (close circles). Solid line from Kondratyuk it et al.[16] and dashed line from Alberico it et al.[17] .

Some approaches assume that the excitation of non- spherical resonances (like the D_{13} and F_{15} resonances) could be affected by the presence of surrounding nucleons, contrary to the case of the Δ resonance which is a simple internal spin-flip excitation of the nucleon. These approaches which can damp the strength of excitation of the higher resonances in nuclei have been recently considered: Giannini *et al.*[18] have predicted a non-negligible damping of the excitation of the higher mass resonances inside the nuclei, using a non relativistic quark model with an oscillator potential that accounts for the quark exchange between the overlapping nucleons (specifically a 11% of damping for D_{13} and 23% for F_{15}) when infra-nucleon distance is about 1 fm. On the contrary, Akulinichev *et al.*,[19] employing a similar non relativistic quark model and short range repulsion to analyze the suppression mechanism for the D_{13} excitation due to the overlap of nucleons, concluded that this effect should be negligible.

2.3. Shadowing region

At energies above the nucleon resonance region ($k > 2$ GeV) the absorption of photons in nuclear matter has been generally considered on vector meson dominance (VMD) assumption, in which the photon interacts with hadronic matter at first converting itself into a linear combination of vector mesons V. The shadowing effect arises when a photon of energy k fluctuates into a vector meson of mass m_V and propagates for a length $l_V = 2k/m_V^2$ close to the nuclear dimension so that there is a non-negligible probability that its interaction is hadronic-like. Earliest simple VMD models[20,21] considered the photon as a superposition of a bare photon and the low-lying vector mesons $V = \rho, \omega, \phi$ and were able to reproduce the photonuclear absorption cross section behavior in the few GeV domain: they predicted a $10 \div 20\%$ shadowing effect around $2 \div 3$ GeV. More sophisticated models (Generalized Vector Dominance)[22,23] included higher mass vector mesons and non diagonal terms in order to better explain higher energy photoabsorption data and virtual photon absorption in deep inelastic electron scattering. Recently Piller *et al.*,[24] assumed, for the intermediate hadronic state, the mass spectral function related to the cross section of the $e^+e^- \rightarrow$ hadrons processes, which include at low energy the $\pi^+\pi^-$ non resonant production and the low energy tail of the broad ρ meson peak. These low mass hadronic components could lower the energy threshold for shadowing which results significant at energy as low as 1 GeV, i.e. in the nucleon resonance region.

Finally, it is worth mentioning that about twenty years ago, Weise provided a sum rule which, employing a dispersion relation approach to reconcile the data for the enhancement factor value observed in the photoabsorption below 140 MeV and the shadowing effect observed above 2 GeV, suggested a strong nuclear medium effect in the whole resonance region.[25]

In order to disentangle from these and other possible explanations, one needs an accurate knowledge of the absolute value of the photoabsorption cross section in the nucleon resonance region, over a broad range of mass numbers.

3. EXPERIMENT

3.1. Beam

The measurements were carried out at Frascati using the jet-target tagged photon beam.[26] A schematic layout of the facility and experimental set-up are shown in Fig.3.

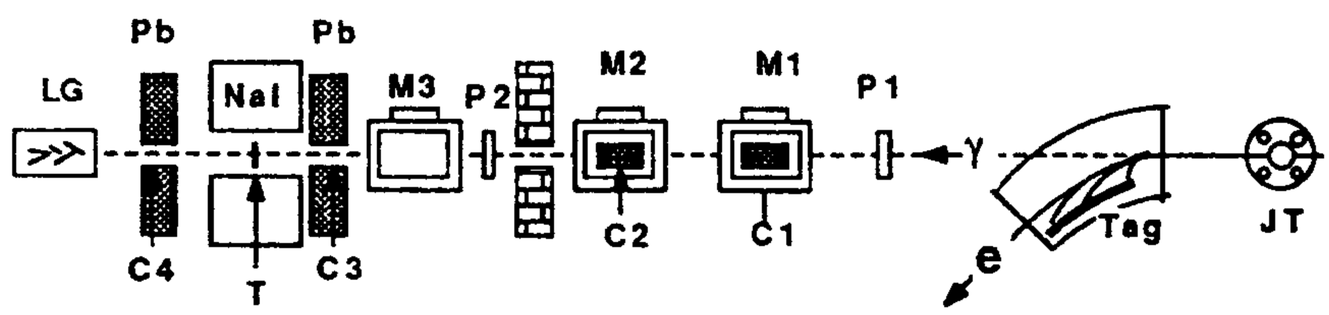

Fig. 3. Layout of the experiment: JT=Jet Target; Tag=tagging system; e=electron beam; γ=photon beam; P1 and P2=beam position monitors; M1, M2 and M3=cleaning magnets; C1, C2, C3 and C4=lead collimators; T=target; NaI=Hadron Detector; LG=Shower Detector.

The photon beam was produced by bremsstrahlung off an argon internal target (JT) of electrons circulating in the ADONE storage ring.[27] The recoil electrons were momentum analyzed by the next dipole and detected by a tagging scintillation hodoscope (T) which covered the photon energy range $0.4E_0 \leq E\gamma \leq 0.8E_0$ (E_0 being the machine energy). Since total cross section measurements didn't require a high photon energy resolution, the tagging channels were hardware summed four by four defining 16 energy channels with a constant energy resolution $\delta E_\gamma / E_\gamma \sim 0.04$.

Along the twenty meter long photon beam line, three cleaning magnets (M1, M2 and M3) swept off the beam the charged particles produced in two movable and variable cylindrical collimators (C1 and C2) and in the windows of the vacuum pipe. The collimators defined a beam spot of 1 cm of diameter on the nuclear target; the beam size and profile were periodically measured with two multiwire proportional chamber (P1 and P2) moveable into and out of the photon beam by remote control.

3.2. Detectors

The total photoabsorption cross section on nuclei was obtained using the photohadronic technique. This technique provided a direct and absolute determination of the photoabsorption cross section by measuring the production rate of hadronic events, and rejecting the preponderant electromagnetic events mainly by an angular separation. In fact, while the hadronic events are more largely distributed in angle, the electromagnetic event distribution is strongly peaked in the forward direction and therefore can be suppressed by using a high efficiency electromagnetic shower detector as a veto counter. This technique was extensively and successfully used in the past for total photoabsorption measurements over a broad photon energy range from the Δ region to 185 GeV.

As a hadron detector (HD) we used a cylindrical NaI crystal anulus (32 cm long, 15 cm thick and 5 cm of internal diameter) surrounding the target. The NaI crystal was segmented into three longitudinal sectors, optically separated by a 1 mm thick aluminum foil. With the target set in the center of the detector, the hadron detection coverage was $9^\circ < \theta < 171^\circ$ for the polar angle and almost 2π for the azimuthal one (which correspond to more than 98% of total coverage in the laboratory system). Each NaI sector was previously calibrated with tagged photons and cosmic rays showing good linearity and homogeneity. Moreover, light emitting diodes (LED) installed on each crystal allowed to monitor regularly the gain stability. A 10 cm thick lead wall was placed all around the HD to shield it from background; moreover a lead collimator (C3), 20 cm long and 3 cm in diameter, placed on the photon beam line before the NaI inner hole, eliminated beam halo effects. The HD provided a good measurement

of the final state total energy for the hadronic event, which was remarkably higher than the one for electromagnetic events in the solid angle defined by the HD detector.

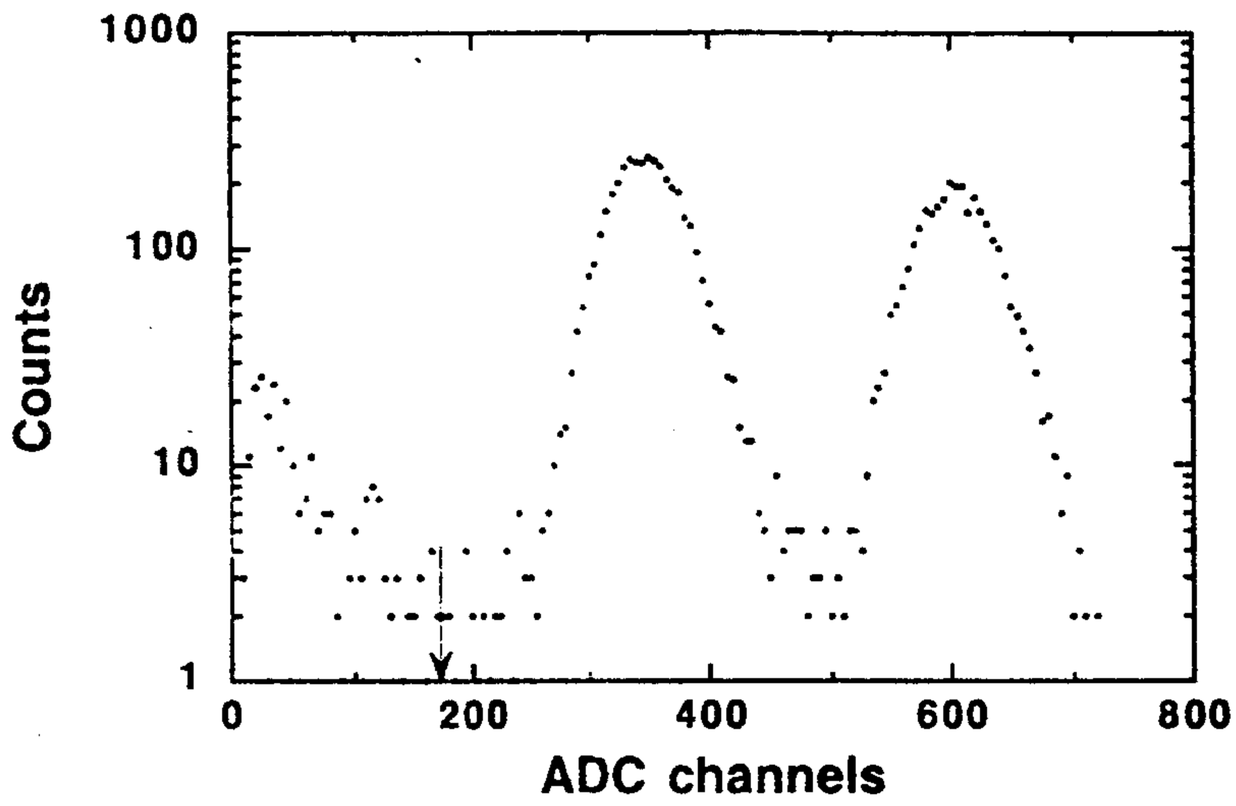

Fig. 4. Response function of the Shower Detector in coincidence with two tagging channels defining photon energies of 340 and 660 MeV. The arrow indicate the threshold setting.

The shower detector (SD) set about 70 cm downstream the target, consisted of a dense SF6 lead-glass cylinder, 30 cm long and 12 cm in diameter, coupled to one 5" photomultiplier. The large detector thickness (19 radiation lengths) provided efficiency equal to one for detecting electromagnetic showers; moreover, its good energy resolution (σ/E) (better than 5% for 1.2 GeV photons) made it possible to set the threshold appropriately and safely. Fig. 4 shows the response of the SD for 343 and 660 MeV tagged photons: as it is seen the two peaks are clearly separated with no low energy tail: the rising of counts in the low channels is due to the random coincidences bremsstrahlung spectrum. The SD response stability was periodically checked by monitoring simultaneously the peak positions of four tagging channels. A lead collimator (C4), 20 cm long and 8 cm diameter, was placed between the HD and the SD for defining a maximum polar angle of 4.2° for electromagnetic events

at the target center. The cerenkov light emission process in the SD ensured also a good rejection of possible low energy hadrons reaching the SD, with a kinematical threshold of $\beta \simeq 0.55$.

3.3. Targets

We used solid targets in the form of circular disks, 3 cm in diameter and thickness (see Table I) about $0.1X_0$ for C, Al, Cu, Sn and Pb and $0.025X_0$ for Li (being X_0 the radiation length). The disks were individually mounted on slides and moved into and off of the photon beam. Due to finite thickness T of the target the effective photon beam was partially attenuated by electromagnetic interaction: specifically the average photon transmission prior an hadronic interaction was given by:

$$\frac{n(T,\mu)}{n(0,\mu)} \cdot = \frac{(1-e^{-\mu T})}{\mu T} \tag{1}$$

where μ is the photon attenuation coefficient. The calculated values of the average photon transmission for this experiment ranged from 99.1% for Li to 96.5% for heavier nuclear targets. Additional runs with different thicknesses ($0.025X_0$ and $0.05X_0$) did not show any additional thickness effect.

Table I : targets, thicknesses, number of collected events # (x10^3) and overall average off-line correction δ for each target and electron beam energy E_0 [GeV].

Target	Thickness	$E_0 = 0.73$		$E_0 = 0.85$		$E_0 = 1.2$		$E_0 = 1.5$	
	[g/cm^2]	#	δ	#	δ	#	δ	#	δ
Li	1.996±0.029			13	10%			18	6%
C	3.452±0.014	25	11%	20	10%	18	7%	19	7%
Al	2.408±0.009	15	12%	12	11%	13	7%	13	7%
Cu	1.272±0.009	10	13%	9	11%	13	8%	11	7%
Sn	0.892±0.007	9	13%	12	11%	11	8%	10	7%
Pb	0.658±0.023	8	10%	10	11%	7	8%	17	8%

In order to reduce possible effects due to changes of stored electron beam, data for all the targets were collected for each fill of the machine and the electrons were always re-injected into the storage ring only after the completion of one or more

measurement cycles. Empty-target measurements were regularly interspersed inside a complete cycle of solid-target runs and then subtracted. The empty-target background yield was roughly equivalent to $\sim 0.8 g cm^{-2}$ of carbon, so that the carbon-target background contributed about 20% of the total event rate. This background was constant in time and could be attributed mainly to electromagnetic events generated upstream the target, from the exit window of the photon beam line and from the air after the sweeping magnet M3 and before the target. It is worth noticing that the stability of all the measurements was about 3%, well inside their statistical error. The target thicknesses together with the number of collected events and the off-line corrections for the different energies are given in Table I.

3.4. Electronics

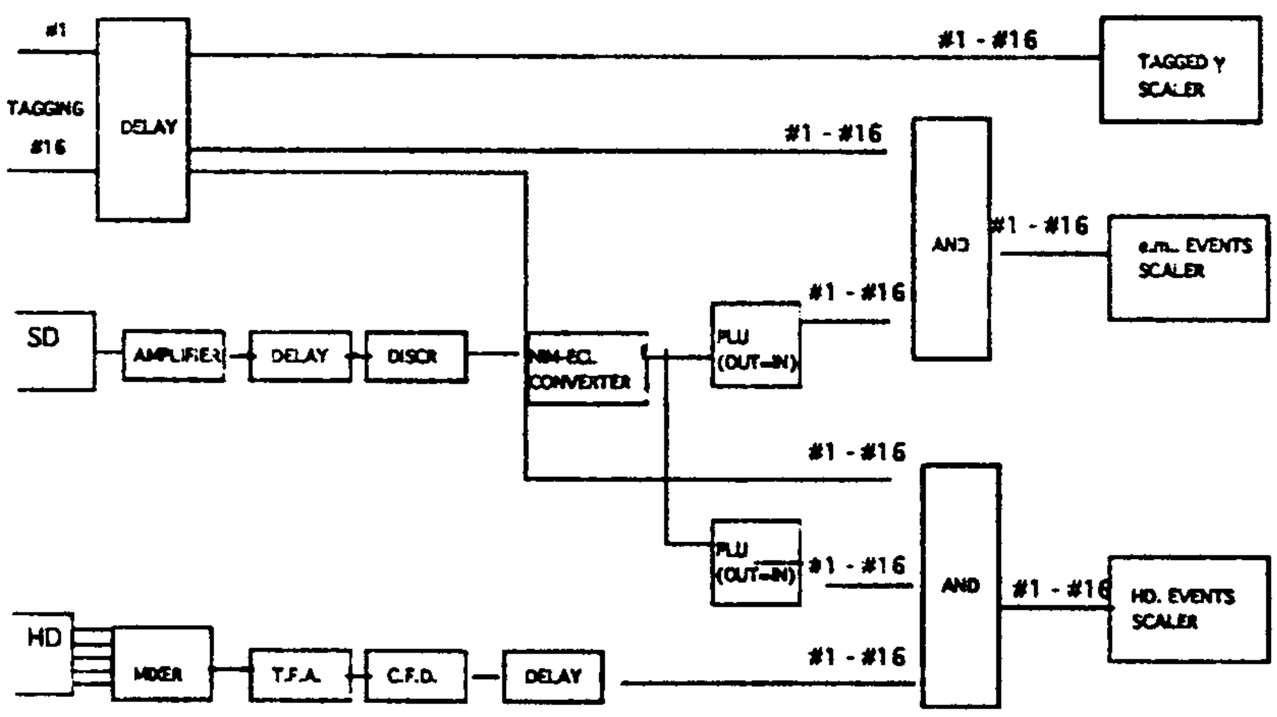

Fig. 5. Electronics diagram.

Fig. 5 shows a block overview of the electronics. The signals from the 16 tagging channels in coincidence with the SD, were recorded on scalers providing the photon beam flux $N_\gamma(k)$. The hadronic events $N_H(k)$ were signed by the coincidence between

the tagging and the HD signals, vetoed by the SD signal above a threshold fixed for each energy. They were also counted with an additional scaler. The random coincidences on both coincidences due to the electron beam time structure were on-line measured and subtracted. After this subtraction we defined an on-line cross section $\sigma_T(k)$, derived from the scaler counts as follows:

$$\sigma_T(k) = \frac{AN_H(k)}{N_A \rho x N_\gamma(k)} \tag{2}$$

where A is the mass number, N_A is the Avogadro number, ρx is the target thickness.

3.5. Measurement

We collected data in several runs distributed over half a year. We covered the photon energy range from 300 MeV to 1200 MeV with four different electron beam energies E_0=1500 MeV, E_0=1200 MeV, E_0=850 MeV, E_0=730 MeV, which ensured large overlapping regions of photon energy. Running conditions, such as HD and SD discriminator threshold settings, were adjusted to optimize the efficiency of hadron detection and of the electromagnetic suppression for the different beam energies: hadron detector equivalent energy thresholds ranged from 27 MeV to 59 MeV, and from 75 MeV to 280 MeV for the e.m. ones. The random to true coincidence ratio was maintained $\sim$ 10% by keeping the tagged photon beam intensity at a constant rate of $\sim 10^4$ photons/s. Moreover we checked the random coincidence on-line subtraction procedure by deriving the on-line cross section at very different photon rates: as it is seen in Fig. 6 no additional rate effect was found when changing the rate of tagged and untagged photons up to a factor of five. Furthermore, the low photon rate as compared with the electron beam bunch rate (51.411 MHz), and the thin radiator thickness ($\sim 10^{-11}$ radiation length), made negligible the probability of two tagged photons in the time resolution of the detector.

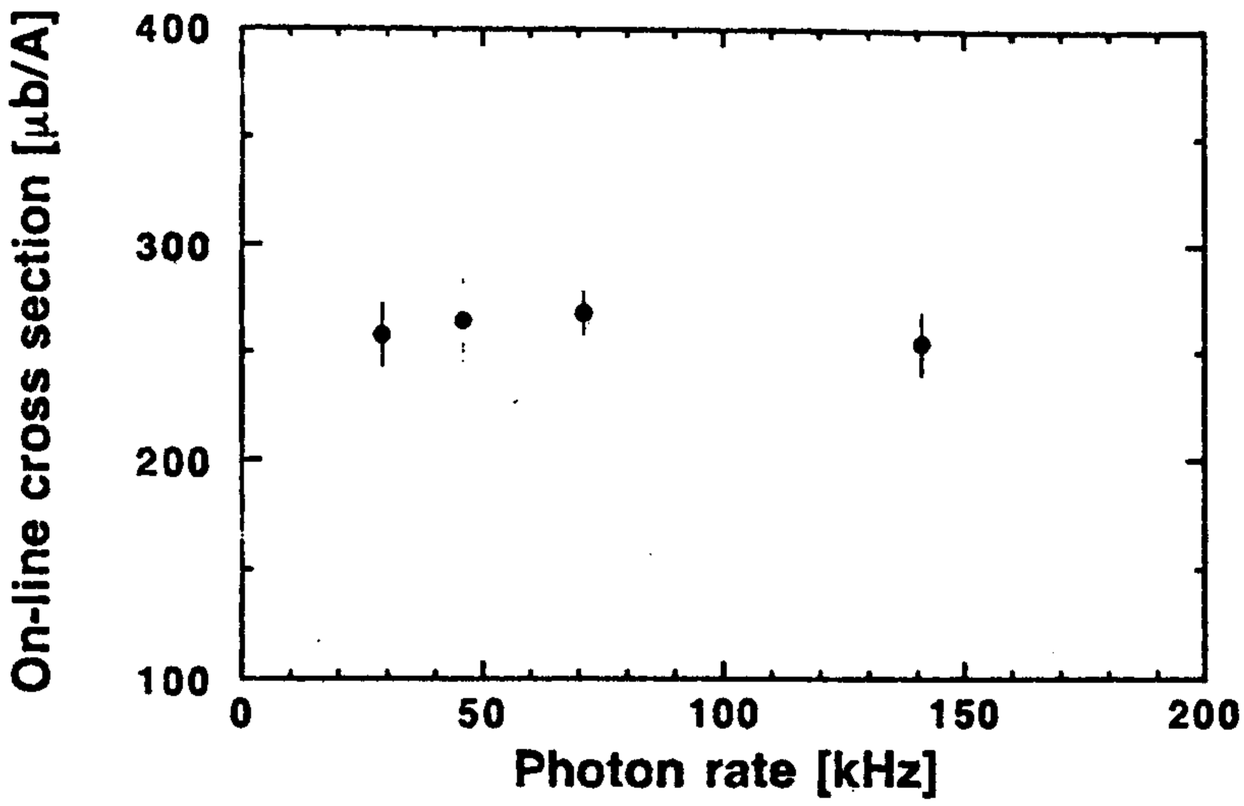

Fig. 6. On-line average cross section for carbon measured with E_0=850 MeV, for different photon total rates.

4. PROCEDURE AND RESULTS

The hadronic technique provided on-line cross section data very close to the absolute values. In fact, small off-line corrections were needed to account for: (i) the loss of hadronic events emitted in the forward hole of the HD or with energy below the HD threshold, (ii) the HD contamination of the electromagnetic events above the HD threshold and not vetoed by the SD and (iii) the loss of hadronic event due to pulse height above the SD threshold simulating an e.m. event.

In order to properly calculate these corrections, particular care was devoted to study the apparatus response function.

Photoproduction of hadronic events on the target, was simulated by using a Monte Carlo program based on a cascade-evaporative model.[28] This code describes the photon interaction with nucleons through the quasi-deuteron process and the one-pion and two-pion production processes in resonant and non resonant states and thus can be applied to the photoabsorption of up to 1.2 GeV photons. Hadrons

photoproduction and residual nucleus excitation are the result of the cascade stage of the photonuclear interaction; successively the excited residual nucleus emits low-energy evaporation nucleons or light nuclei.

The response function of the hadron detector to the generated hadronic events. was studied with a Geant-3 code modified to correctly take into account the hadronic cross section in NaI for protons, neutrons and charged pions and also by supplying the energy-range tables in NaI for protons and pions at energies below 1 GeV.[30] Fig. 7 shows the comparison between the HD simulated and measured response functions to the hadrons photo produced on C by $600 \div 1200$ MeV photons. The good agreement between the Monte Carlo prediction and the measured spectrum, ensured a good estimate of the correction due to the hadronic losses below the HD threshold.

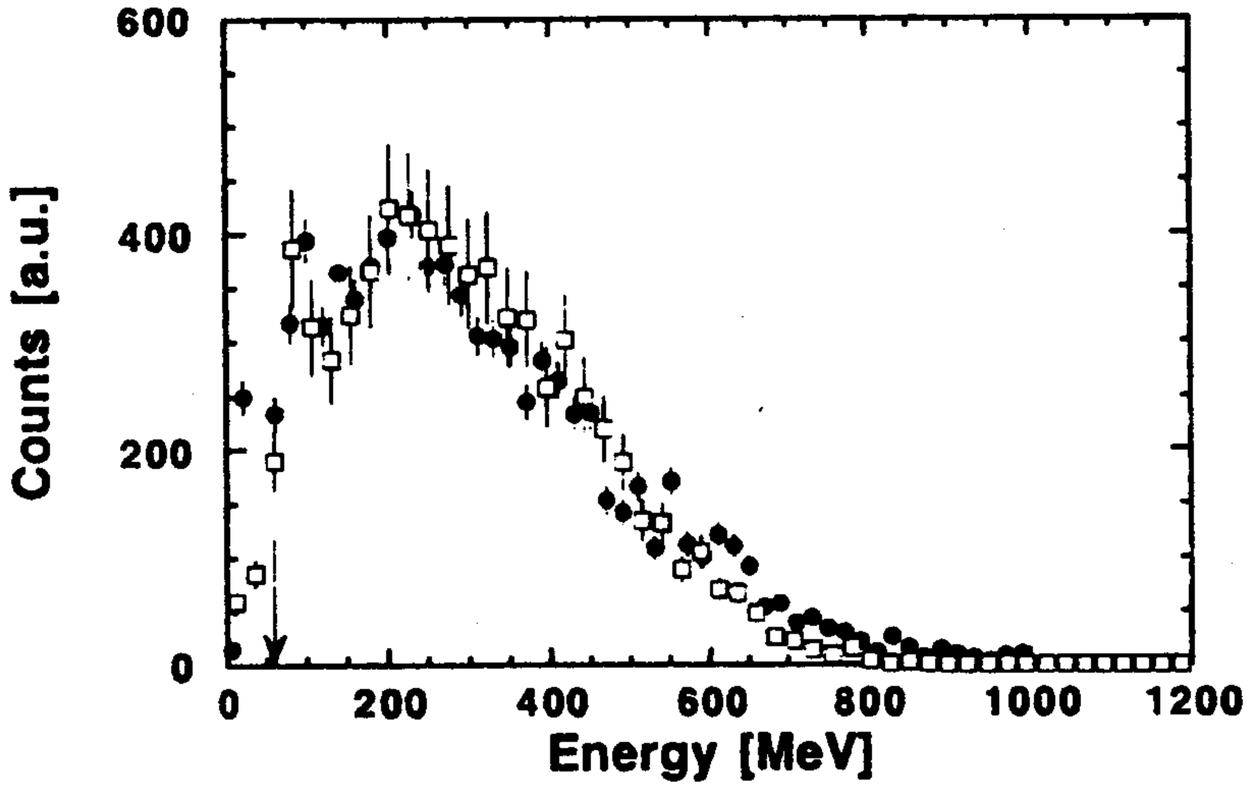

Fig. 7. Comparison between the simulated (open squares) and measured (close circles) response function of the Hadron Detector to $600 \div 1200$ MeV photons on carbon target. The arrow indicates the threshold setting.

We also simulated the electromagnetic processes with a modified version of the Geant- 3.13 code which correctly accounts for the measured angular distribution of pair production in the energy range of interest both in nuclear and atomic field, while

the standard Geant 3.13 code assigned to the polar angle θ the approximate average value $\theta = m/k$, where m is the electron mass and k is the photon energy. Moreover, we also implemented the Geant 3.13 code with the Cerenkov photons emission, the attenuation in the lead glass of the Cerenkov light, and the spectral response of PMT.

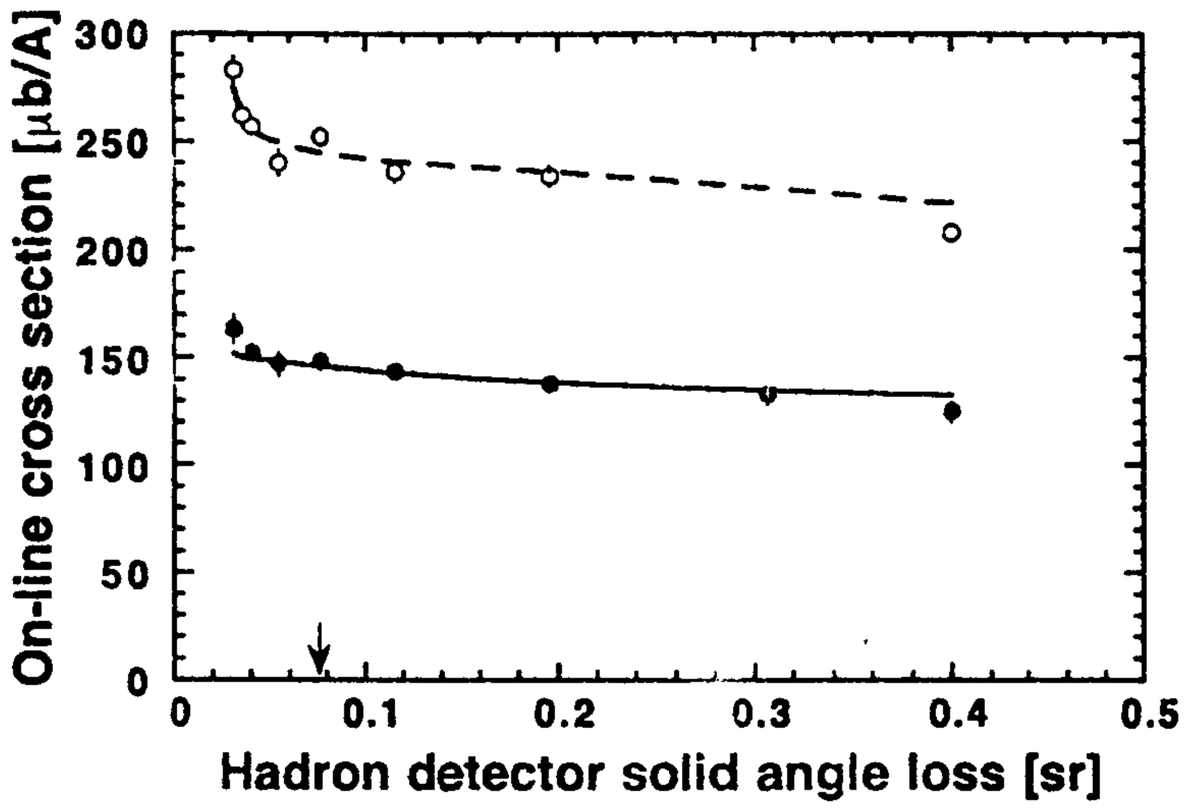

Fig. 8. The on-line average cross section measured on the tin target for two electron beam energy with different solid angle coverage of the HD. Open and full circles refer respectively to E_0=850 MeV and E_0=1500 MeV measurements. The dashed and the solid lines are the relevant MC predictions. The arrow indicates the measurement position.

Monte Carlo corrections for the finite angular acceptance of the HD and for the possible contamination due to the electromagnetic events not vetoed by the SD, were experimentally tested by changing the HD solid angle; this was performed by moving upstream and downstream the targets inside the HD. Fig. 8 shows the on-line average cross section values measured at two beam energies ($E_0 = 1.5$ GeV and $E_0 = 0.85$ GeV) for different tin-target positions, as a function of the uncovered forward solid angle, $2\pi\theta^2$ (hole), of the HD. The arrow indicates the missing solid angle that corresponds to the standard position used for cross section measurements with the target placed in the center of the HD. The Monte Carlo predictions are

parametrized by a curve $a - b\theta^2 + (c/\theta^2)$, where a is the total hadronic cross section for an ideal 4π hadron detector, $-b\theta^2$ represents the loss of hadronic events in the forward hole of the HD, and $+c/\theta^2$ represents the contamination of electromagnetic events due to the pairs produced in the target. As shown, the latter becomes relevant only when the target is moved very upstream to positions which correspond to very small θ^2 values and the HD solid angle coverage approaches 4π. The values deduced from this measurement for both these corrections well agree with the predictions of the Monte-Carlo calculations.

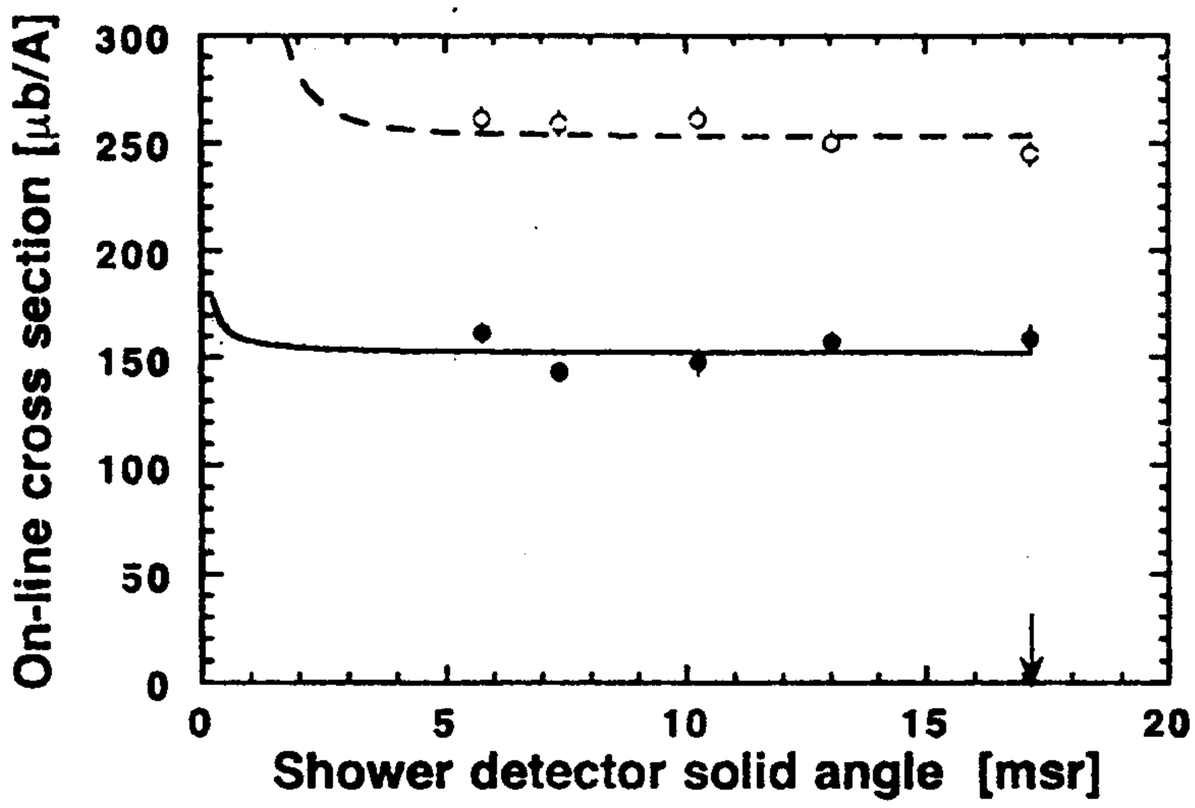

Fig. 9. Same of Fig. 8 but with different solid angle coverage of the SD. The arrow indicates the measurement position.

The rejection efficiency due to angular acceptance of the SD was also evaluated by changing the radius of the C4-collimator and compared with the Monte Carlo prediction. Fig. 9 shows the on-line average cross section data on a tin-target measured at two electron beam energies (E_0=1.5 GeV and E_0=0.85 GeV) as a function of the forward solid angle covered by the SD. The arrow indicates the standard solid angle for the cross section measurements. The two curves, that represent the Monte Carlo

predictions, are parametrized in the form $a+c/\theta^2$ and well agree with the experimental points. As it is shown the hadronic cross section a is constant in a wide range of forward angles thus indicating that the electromagnetic events were adequately and safely suppressed by the veto counter. The increase of the cross section predicted for small angles ($+c/\theta^2$ term) is ascribed to the low energy showers, generated inside the C4-collimator, which produce a signal below the SD veto threshold.

The good agreement between the Monte Carlo predictions and the experimental results confirms a high reliability of the calculated corrections for both the hadronic and electromagnetic events. Moreover it is worth noticing that the electromagnetic contamination correction has the opposite sign with respect to the hadronic loss correction, and this results into a reduced total absolute software corrections to the on-line results. Table I lists the average value of the Monte Carlo corrections with respect to the on-line values, for different energies and for all the studied nuclei.

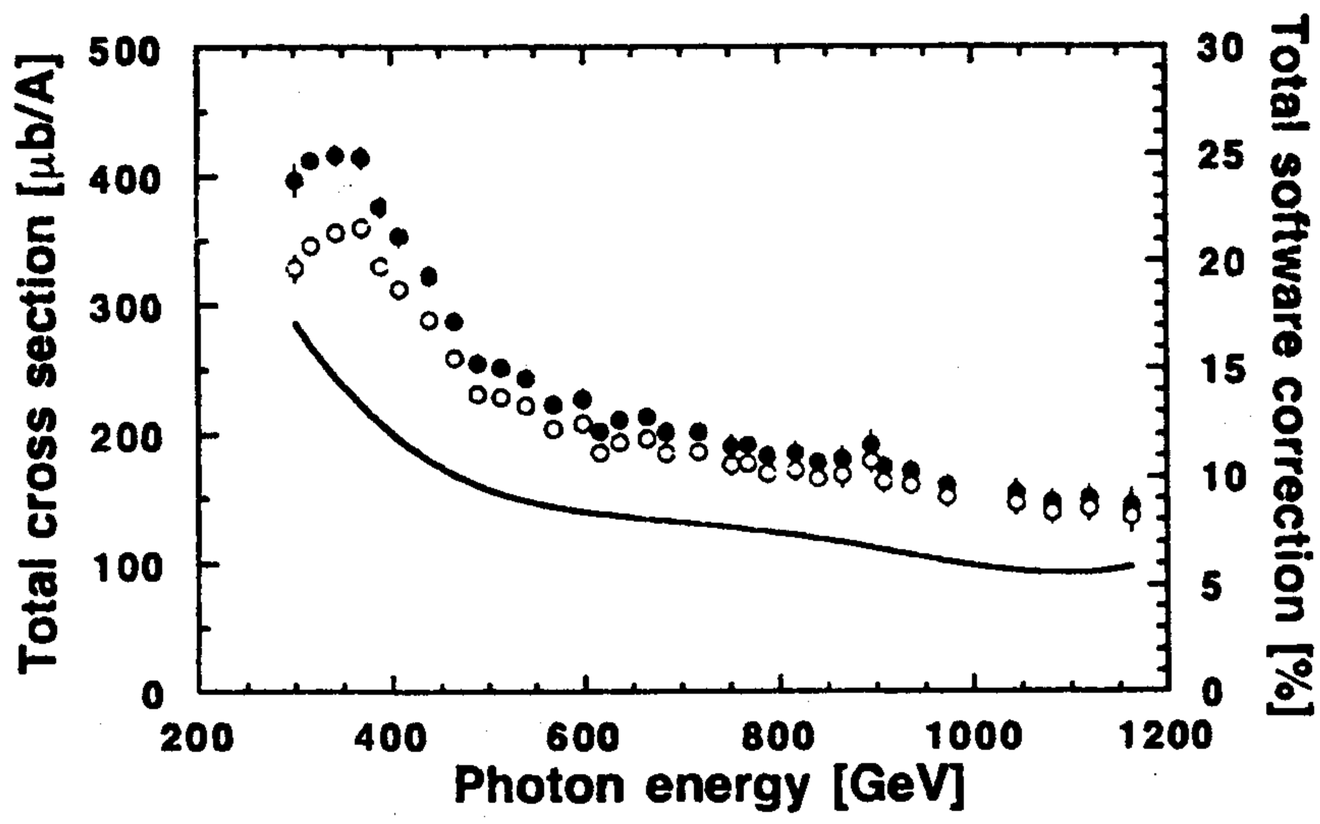

Fig. 10. Aluminum on-line (open circles) and off-line (close circles) total cross section (left scale) and the amount of the total correction (rigth scale) due to hadronic losses and electromagnetic contamination on the on-line data (solid line).

In Fig. 10 the comparison between the on-line and off-line cross section is shown for the aluminum target, together with the absolute software corrections behavior in the whole photon energy range. As it is seen the total correction decreases from about 15% to about 5% while the energy increases.

In Table II are given the final total cross section values normalized to the mass number A for the six studied nuclei together with the statistical errors. Also given is the weighted average of data points which can be considered as the cross section on an "average" nucleus with $Z/A = 0.465$, $N/A = 0.535$, density $\rho = 0.101 nucleons/fm^3$ and Fermi momentum $p_F = 232 MeV/c$, i.e. an "aluminum-like" nucleus. Plot of these data are shown in Fig. 11 with statistical errors only, while systematics errors are represented by the bands in the bottom.

The good overlaps observed between the data collected at different energy sets, evidenced the good control of the systematic errors. These were essentially due to uncertainties in the photon beam flux ($\simeq 2\%$), the target thickness ($\sim 0.5 \div 1.5\%$) and mainly the calibration and threshold efficiency of both the shower and hadron detectors (above 600 MeV this contribution is constant with energy and increases from $\simeq 2\%$ to $\simeq 6.5\%$ with the target mass number A, while, in the Δ region , where it depends both on energy and A, it varies from $\simeq 4.5\%$ to $\simeq 7.5\%$). In conclusion, the total systematic errors increase with A from $\simeq 3\%$ to $\simeq 7\%$ in the D_{13} and F_{15} resonance regions and vary from $\simeq 5\%$ to $\simeq 8\%$ in the Δ region.

Table II : total cross section values normalized by the mass number A for each nucleus. Also indicated are the statistical errors. The average is computed weighting each nucleus cross section datum with its statistical error.

k [GeV]	^{7}Li [μb/A]	C [μb/A]	Al [μb/A]	Cu [μb/A]	Sn [μb/A]	Pb [μb/A]	Average [μb/A]
0.301		420±10	397±13	375±16	398±19	387±21	401.5±6.5
0.317		430±7	412±9	430±12	419±14	381±15	419.5±4.6
0.343	440±15	432±6	416±8	403±10	417±11	415±12	421.2±3.6
0.369	389±10	406±6	414±8	413±13	413±10	410±12	407.1±3.6
0.389	351±12	393±6	376±8	376±8	399±11	389±10	383.6±3.4
0.408	324±13	362±7	353±9	358±12	378±13	329±14	354.7±4.1
0.439	282±9	324±6	323±7	317±9	328±10	337±15	317.8±3.3
0.465	257±13	287±5	288±7	294±9	322±10	319±12	292.0±3.2
0.490	244±12	251±5	255±7	252±8	250±9	257±11	251.6±3.2
0.514	223±12	254±4	251±5	247±6	241±8	273±9	250.9±2.5
0.540	194±7	235±3	243±4	236±5	245±6	249±7	235.7±2.0
0.568		216±6	222±7	219±9	228±11	240±13	221.1±3.6
0.598	222±11	218±6	227±7	212±9	222±10	210±12	218.8±3.4
0.616	211±6	200±5	202±6	197±8	210±9	197±8	202.6±2.7
0.636	196±6	210±4	211±5	201±6	203±7	192±8	204.2±2.3
0.664	213±7	207±4	213±5	198±7	207±7	191±7	206.4±2.2
0.684	205±7	190±6	201±8	192±7	181±10	174±9	192.4±3.0
0.717	206±8	185±5	201±6	186±7	171±9	173±9	188.4±2.7
0.751	194±9	181±7	190±9	175±10	207±9	159±12	186.0±3.6
0.768		195±5	191±6	179±8	178±13	187±12	189.8±3.2
0.788	166±7	184±7	183±9	174±12	173±13	173±12	176.3±3.6
0.817	180±9	183±7	185±9	163±12	187±14	178±12	180.3±3.9
0.840	194±8	187±5	178±6	179±8	180±10	182±11	183.7±3.0
0.865		181±8	180±10	172±12	179±16	218±21	181.1±4.9
0.895		182±7	192±10	164±12	169±15	195±14	181.3±4.7
0.908	169±8	162±7	174±9	169±13	182±12	167±15	169.1±3.9
0.936	137±7	166±5	171±7	160±10	162±13	168±12	160.3±3.2
0.973	171±8	178±7	161±9	157±12	151±13	171±12	168.2±3.8
1.044	145±9	167±7	155±9	164±13	158±15	151±14	157.2±4.1
1.081	165±10	147±7	147±10	148±15	148±17	147±15	150.9±4.4
1.119	147±8	156±7	150±10	143±14	154±16	163±15	151.6±4.1
1.163	140±12	144±10	144±13	145±20	120±22	135±20	140.7±5.7

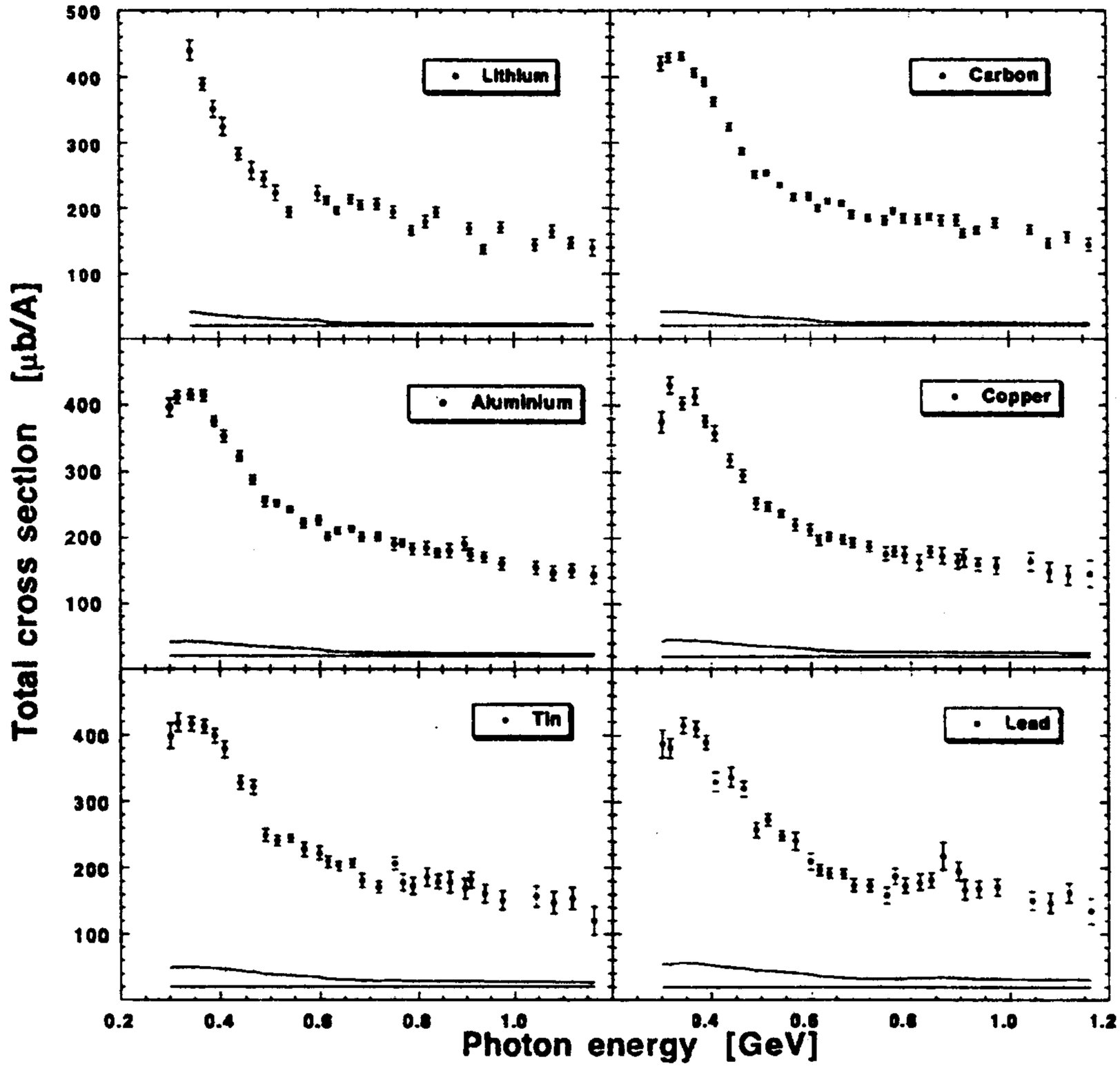

Fig. 11. Total cross section for the six nuclei. The error bar represents the statistical error. The band at the bottom of each plot represents the systematic error.

5. ANALYSIS AND DISCUSSION

Total photonuclear cross sections can be considered as a convolution of resonant and non-resonant production processes on individual nucleons smeared by nuclear medium effects. To extract informations on the latter ones, we adopted the phenomenological procedure previously used by some of us[16] : we first determine the resonance masses widths and excitation strength by fitting the proton and neutron data, then we fitted the nuclear data using the same analytical expression with some free parameters. With respect to previuos procedure we adopted the following improvements: we used a better Breit-Wigner parametrization of the resonances, a more accurate determination of neutron cross section values from the deuteron data, a different non-resonant pionic background parametrization and more precise nuclear densities. Moreover we also considered in nuclei the contribution of quasi-deuteron background, of nuclear effects (like resonance mass shifts and suppression) and the shadowing effect.

5.1. Free nucleon parametrization

In order to determine the resonance masses W_r, widths Γ_r and strengths I_r, we fitted the proton data available in the literature[9,31] to a sum of six Breit-Wigner plus a smooth background The six resonances parametrized in the fit can be identified as the $P_{33}(1232)$ (Δ-resonance), $P_{11}(1440)$, $D_{13}(1520)$, $S_{11}(1535)$, $F_{15}(1680)$ and $F_{37}(1950)$, which give the main contribution to the total γN cross section. We expressed the Breit-Wigner resonances in the form given by Walker[32] which is correct at least for the one pion decay channel:

$$I = I_r(\frac{K}{K_r})^2 \frac{W_r^2 \Gamma \Gamma_\gamma}{(W^2 - W_r^2)^2 + W_r^2 \Gamma^2} \tag{3}$$

where

$$\Gamma = \Gamma_r(\frac{q}{q_r})^{2l+1}(\frac{q_r^2 + X^2}{q^2 + X^2})^l \tag{4}$$

$$\Gamma_\gamma = \Gamma_r(\frac{K}{K_r})^{2J\gamma}(\frac{K_r^2 + X^2}{K^2 + X^2})^{J\gamma} \tag{5}$$

and W is the c.m. energy; K and q are the momenta of the photon and single pion decay in the c.m. frame, and the suffix r refers to the values at the resonance mass W_r; J_γ and l are their angular momenta. The damping parameter X for free protons was set equal to 0.35 GeV for all the resonances except for the Δ for which the value X=0.15 was used.

To take into account the non-resonant pion production, we considered in the fit also a background parametrization of the simple form:

$$\sigma_B = (a_1 + a_2 k^{-1/2})(1 - e^{-2(k-k_0)}) \tag{6}$$

which has the correct Regge energy asymptotic behavior and include the pion photoproduction threshold energy k_0. The values a_1 and a_2 were fixed by matching with the results of high energy data ($k \geq 2$ GeV)[9] resulting for the proton $a_1^p = 91\mu b$, $a_2^p = 71\mu b GeV^{1/2}$. The fit function is therefore expressed by:

$$F = \sum_r I(I_r, W_r, \Gamma_r) + \sigma_B(a_1, a_2) \tag{7}$$

In fig. 12a) it is shown the comparison between data on proton and the fit, together with the single contributions of the different resonances and background.

In order to extract the total cross section on free neutron we performed a fit to the deuteron data.[10,31] In this fit we used the same parametrization as for the proton plus an additional non-resonant photodisintegration cross section background which gives a non negligible contribution mainly in the Δ region; this has been extracted from total photodisintegration cross section and the result well agree with the theoretical prediction which include Meson Exchange Current with no Isobar terms.[33] More details about this non-resonant photodisintegration contribution will appear in a forthcoming paper. The non-resonant pionic background parameter resulted for the deuteron $a_1^D = 175\mu b$, $a_2^D = 135\mu b GeV^{1/2}$ and were derived from high energy data.[10] Moreover we assumed that the resonance parameters W_r and Γ_r for the neutron do not change respect to the proton case, that is $W_r^n = W_r^p$ and $\Gamma_r^n = \Gamma_r^p$. On the contrary, the resonance couplings I_r, which in principle could be different, were derived

from deuteron and proton resonance parameters as follows:

$$I_r^n = \frac{I_r^D \Gamma_r^D - I_r^p \Gamma_r^p}{\Gamma_r^n} \tag{8}$$

Then the neutron cross section has been calculated from the experimental deuteron and proton data:

$$\sigma^n = \sigma^d \frac{F^p + F^n}{F^D} - \sigma^p. \tag{9}$$

This is shown in Fig. 12b) together with the fit performed on the neutron data.

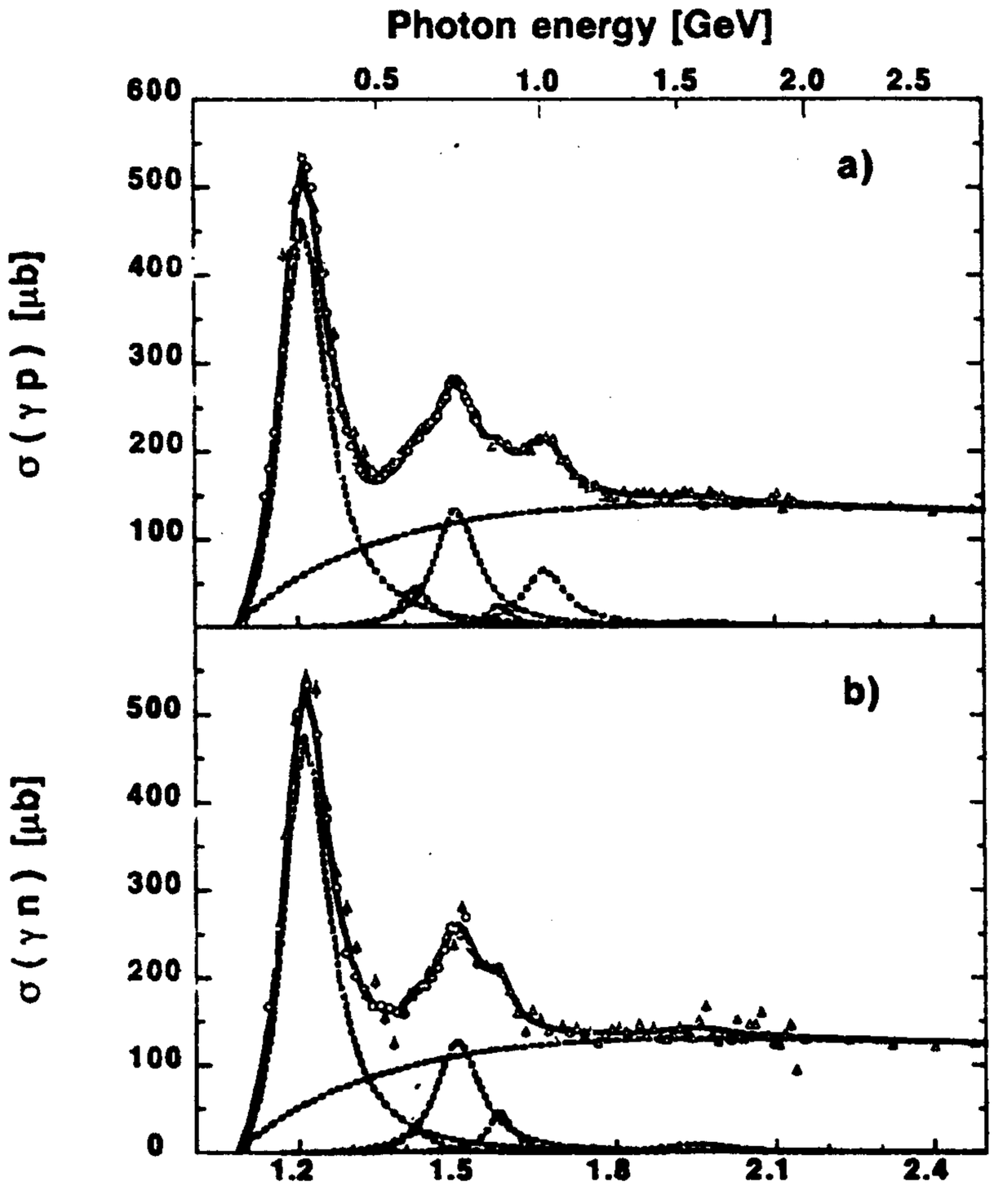

Fig. 12. a) Total cross section measured on proton: open circles[31] and triangles.[9] The solid line is the result of our fit; the dotted lines are the resonant and non-resonant contributions. b) the same for the neutron; neutron data are derived with the procedure described in the text.

The resonance parameters W_r, Γ_r and I_r deduced from the proton and deuteron fits and I_r derived for the neutron are shown in Table III.

Table III : resonance masses W_r, widths Γ_r and strengths I_p for proton (p), neutron (n) and deuteron (d) derived from the hydrogen and deuterium data. Masses and widths for neutron have been assumed equal to the proton ones.

Resonance	W_r [MeV]		Γ_r [MeV]		I_r [μb]		
	p	n	p	d	p	n	d
$P_{33}(1232)$	1230	1241	122	161	415	429	639
$D_{13}(1505)$	1505	1502	100	134	133	128	195
$F_{15}(1680)$	1671	1680	100	110	65	0	59
$P_{11}(1440)$	1423	1413	66	81	47	25	59
$F_{37}(1950)$	1954	1974	150	165	5	8	12
$S_{11}(1535)$	1580	1570	50	73	27	49	52

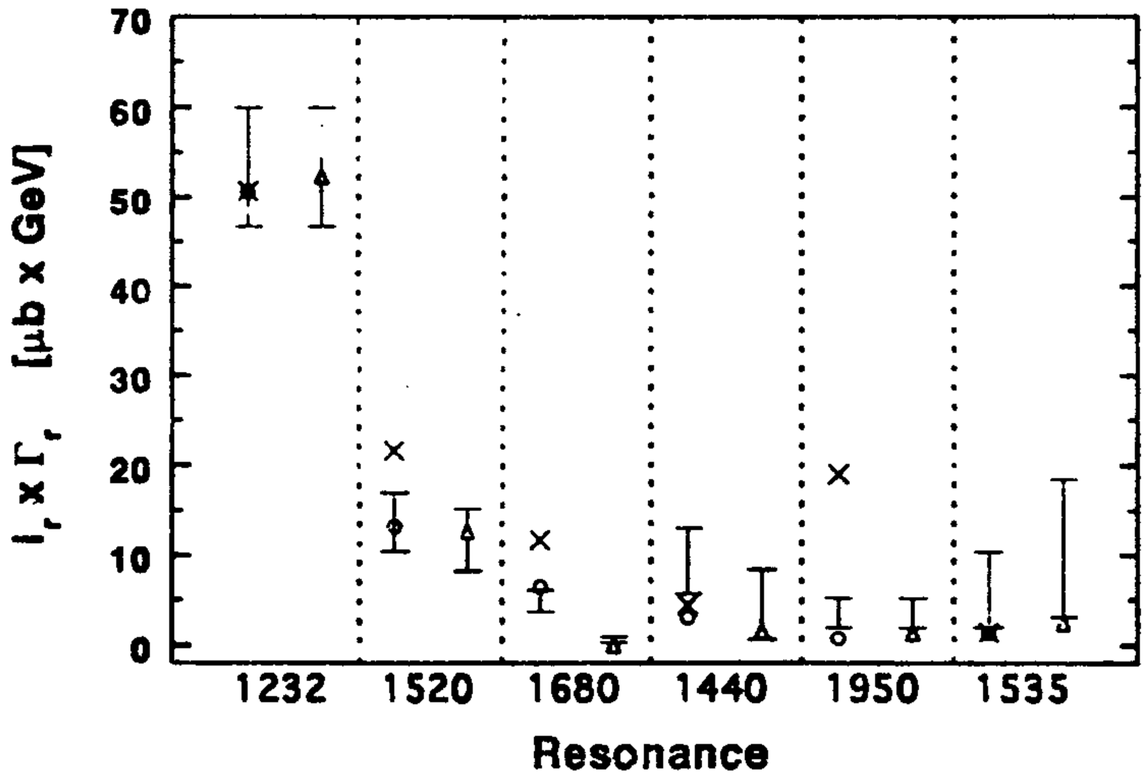

Fig. 13. Areas of the main six nucleon resonaces computed as the product of the strength at the mass by the width. Open circles are the values we derived from fitting data for the proton,[31,9] open triangles are values we derived for the neutron,[31,10] crosses were the values previously derived[9] for the proton and vertical lines are the PDG range.

Fig. 13 shows the integrated strength $\Gamma_r I_r$ values for proton (open circles) and neutron (open triangles) provided by our fit, together with the values calulated by

Armstrong *et al.* for the proton[9] (crosses) and the ranges given by the Particle Data Group[34] (vertical solid line). This comparison shows a general good agreement between the values obtained from our fit and the PDG predictions and point out theimprovement respect to the Armstrong *et al.* results for resonances higher than the Δ. Moreover, we found that the Δ and $D_{13}(1520)$ resonances are approximately equally excited on proton and neutron, while the $F_{15}(1680)$ amplitude is strongly suppressed in the neutron in agreement with the quark model predictions for the electromagnetic coupling of the resonances. The remaining three resonances are less excited and less well defined. Their parameters are more dependent on the background parametrization but their values are still consistent with the PDG values. The mass of $S_{11}(1535)$ is significantly higher compared with the predicted value, nevertheless this resonances was included into the fitting procedure to account for the small enhancement in the proton data at a photon energy of 900 MeV, reducing about of 20% the total χ^2.

5.2. Nuclear medium effects

The resonance parameters obtained from the fits to the free nucleon data shown in Table III are a suitable input for the fit to the bound nucleon data. In order to extract information about the resonance behavior in nuclei, we considered the following processes:

(i) The quasi-deuteron process was parametrized using the Levinger expression[35]:

$$\sigma_{QD} = L\frac{NZ}{A}e^{-D/k}\sigma_D \tag{10}$$

where k is the photon momentum, L is the Levinger factor, $D = 0.06$ GeV is a damping factor and σ_D is the non-resonant photodisintegration cross section on the deuteron. Within this parametrization isobar degrees of freedom are included in the Breit-Wigner term only.

(ii) The Fermi motion, which produces a smearing of the resonance peak by increasing its width and suppressing its maximum of a quantity S_F depending on the Fermi energy of the nucleus ($\epsilon_F = 20 \div 40$ MeV). This approximation has been

shown to be valid in the description of nucleon resonances in nuclei where the peaks are hundreds of MeV broad, that is about one order of magnitude bigger than the kinetic energies of nucleons inside the nucleus.[16] This effect has found to increase the resonance total widths in nuclei of about $10 \div 15\%$.

(iii) The Pauli blocking, which arises because of the occupation by other nucleons of the momentum space below the fermi momentum, thus reducing the space phase available for the resonance decay products. This effect increases the resonance lifetime and decreases its width of a quantity B_P identified with the solid angle formed in the resonance rest frame by the allowed nucleon directions.[16] For an average density nucleus, B_P is computed to be 0.77 for the Δ and about 0.90 for higher resonances.

It is to point out that the ii) and iii) contributions partially compensate for each resonance.

(iv) The propagation and interaction of the resonance in the nuclear medium, which reduces the lifetime of the photo-produced resonance thus increasing its width.

In analogy with the Δ propagation in nuclei, the medium effects on the resonance propagation are described by a phenomenological potential whose real and imaginary parts are related to the shift of the mass δM and to the broadening $\delta\Gamma$ of the resonance. Introducing an optical pseudopotential for the N^*N interaction, δM and $\delta\Gamma$ are proportional to the real and imaginary part of the forward N^*N scattering amplitude $f_{N^*N}(0)$ and to the density of the nuclear medium ρ_0:

$$\delta M = -\frac{2\pi}{M} Re f_{N^*N}(0)\rho_0 \tag{11}$$

$$\delta\Gamma = \frac{4\pi}{M} Im f_{N^*N}(0)\rho_0. \tag{12}$$

Using the optical theorem we deduced :

$$\delta\Gamma = \rho_0 \sigma^* v\gamma \tag{13}$$

where v is the propagation velocity, γ is the Lorentz factor and σ^* is the total cross section of the resonance-nucleon interaction.

A more details of these nuclear effects and their influence on the resonances behavior in the nuclear medium, have been described elsewhere..[16]

Taking into account the above listed processes, each resonance in the nuclear medium was parametrized by a total broadening Γ and mass M:

$$\Gamma = \frac{\Gamma_r B_P + \delta\Gamma}{S_F} \tag{14}$$

$$M = W_r + \delta M \tag{15}$$

Moreover, in the Breit-Wigner expression we decreased the damping parameters X given in eq. (4) and (5) in order to properly take into account the resonance broadening in the nuclear medium.

In the fits to the total cross sections on nuclei we used W_r, Γ_r and I_r obtained from the fit to the proton and neutron data, the computed values for B_P anf S_F while $\delta\Gamma$ (or $\sigma^* v$) and δM were free parameters. In order to decrease the total number of free parameters we assumed $\delta M = 0$ for all the resonance except for the Δ. This because the Δ in the nuclear medium is dominant and much narrower than the other resonances and even a small shift of its mass contributes very significantly to the χ^2 value. Moreover, we used as free parameters only two $\delta\Gamma$ (or $\sigma^* v$): one for the $P_{33}(1232)$ resonance and a common one for all other resonances. As our data cover the mass range between $1.20 < W < 1.75$ GeV, in order to complete the whole $P_{33}(1232)$ energy region, we used data available from previous experiments in the range $1.14 < W < 1.20$ GeV, where the lower limit is the same of the proton and neutron data fit. Specifically, we used lithium data[36] for lithium, carbon data[37,38] for light nuclei, and lead data[38] for heavy nuclei. The results of the fit to the average nucleus total cross sections are shown in Fig.14 together with the separate resonant, quasi-deuteron and background contributions. As it is seen the fit reproduces quite well the data. The best description of the data was found for $\delta M_\Delta = 38 \pm 1$ MeV and $\sigma^* v_\Delta = 35 \pm 1$ mb, for the Δ resonance and $\sigma^* v_{N^*} = 135 \pm 5$ mb in average for the other N^* resonances. While the $\sigma^* v_\Delta$ value is in fair agreement with the one derived from the $NN \rightarrow \Delta N$ processes, the value found for the other resonances violate the unitarity limit which requires $\sigma^* v_{N^*} \leq 80$ mb.[16]

To better investigate broadening or shift of resonance structures is usefulto study the ratio of the bound nucleon to free nucleon cross sections which is a pa-

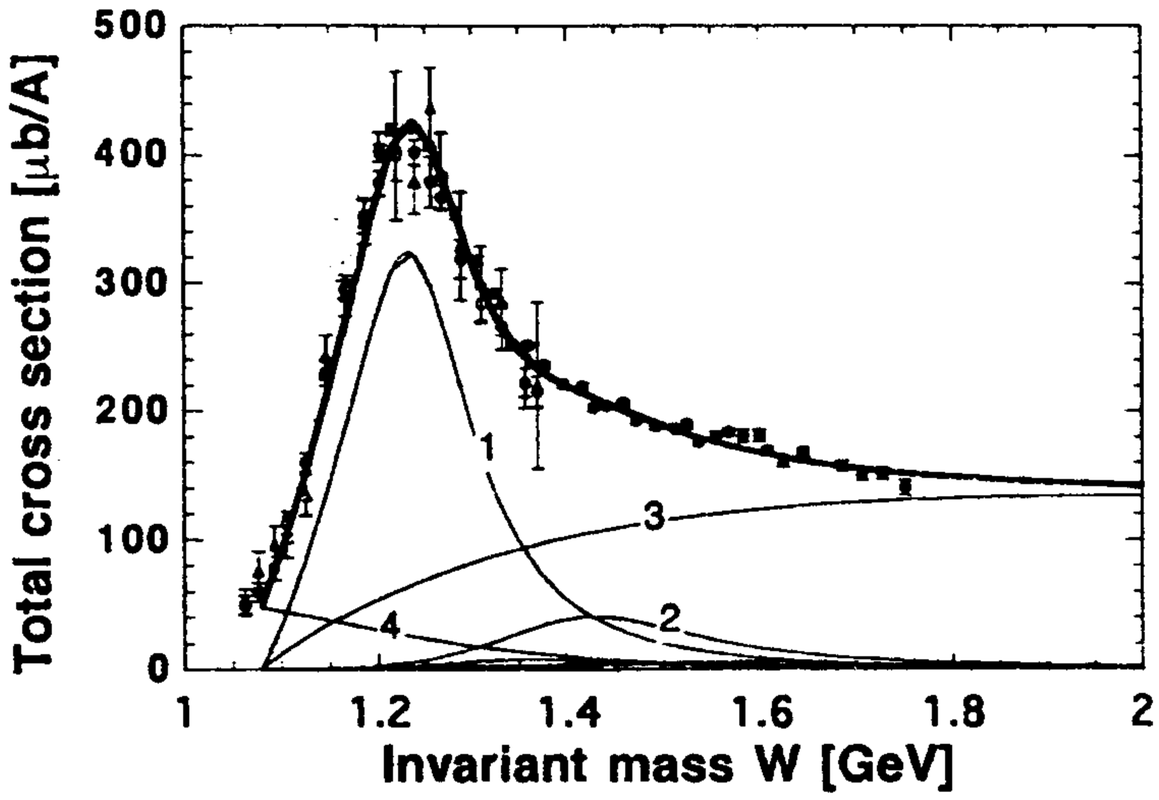

Fig. 14. Total cross section data: our data on the average nucleus (close circles) are compared with previous data on C (open circles) and Pb (open triangles) measured with a similiar experimental technique.[38] Also shown is our phenomenological fit (thick line) with resonant and non-resonant separate contributions (thin lines) of the P_{33} (1) and D_{13} (2) excitation, pionic background (3) and quasi-deuteron background (4).

rameter strongly dependent of these effects. In particular either a broadening or a shift produce an oscillating behavior of the ratio. Fig.15a shows the ratio between the measured average nuclear data and the fit to the free nucleon, together with the ratio computed with the above described model. Also shown are the prediction of the model in the case of no shift for the Δ ($\delta M_\Delta = 0$) and no broadening ($\delta\Gamma = 0$) due to the resonance interaction (Pauli blocking and Fermi motion only): as it is seen propagation and interaction of resonances are really needed to explain the data up to 1.2 GeV. Moreover, from the figure it appears that the used resonance broadening leads to an antishadowing behavior at higher energies with a large overestimate above 2 GeV.[39]

These problems like the violation of the unitarity limit and the antishadowing behavior can be solved only introducing an effective reduction of the cross section in

the resonance region. Two effects have been introduced to justify this reduction:

i) the existance of a dynamical mechanism which inhibits the excitation of nucleon resonances in nuclei, causing a reduction of I_τ in nuclei.[18]

ii) the onset of nuclear shadowing,[40] which causes a reduction of the total cross section. It is worth to point out that in the framework of this model no resonance effects are considered.

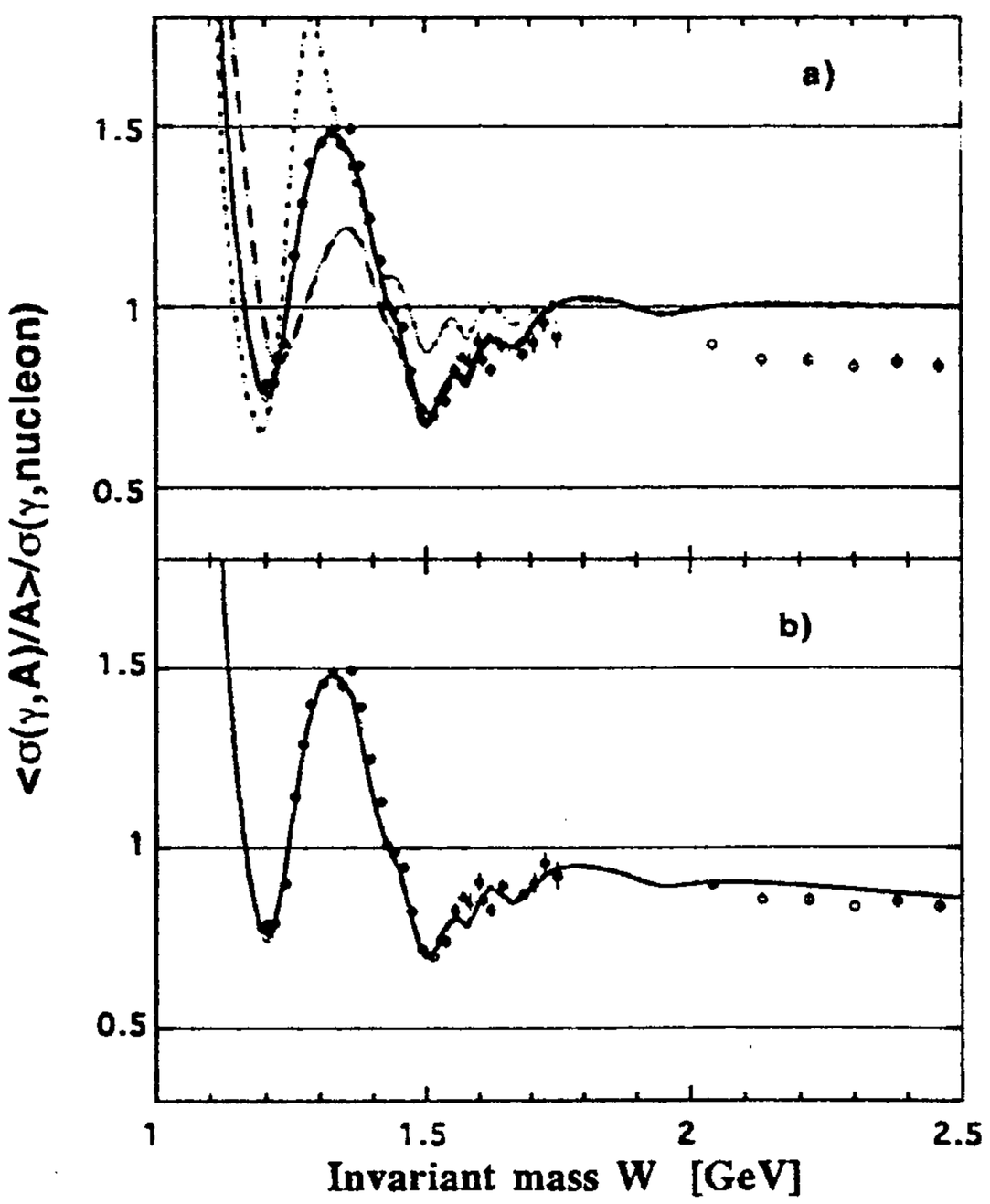

Fig. 15. a) Ratio between cross section on the average nucleus and that on a free nucleon: our data are indicated by the close circles while Daresbury data[39] by open circles. Solid line is the result of our phenomenological model described in the text which consider Fermi motion, Pauli blocking and resonance propagation and interaction; dashed line is the result of the model when imposing $\delta M_\Delta = 0$ (no Δ mass shift) while dotted line when imposing $\delta\Gamma = 0$ (no resonance interaction). b) The same of a) but now solid line is the phenomenological model with the inclusion of partial damping of resonances and shadowing effect.

Solid line of Fig. 15b shows how the inclusion of these two effects makes it possible to cure the discrepancy with data at high energy. Moreover, in this case, the cross section ΔN remains almost unchanged, being $\sigma^* v_\Delta = 34 \pm 1$ mb, while the one for higher resonance is strongly reduced, resulting $\sigma^* v_{N^*} = 80 \pm 4$ mb in reasonable agreement with the unitarity limit.

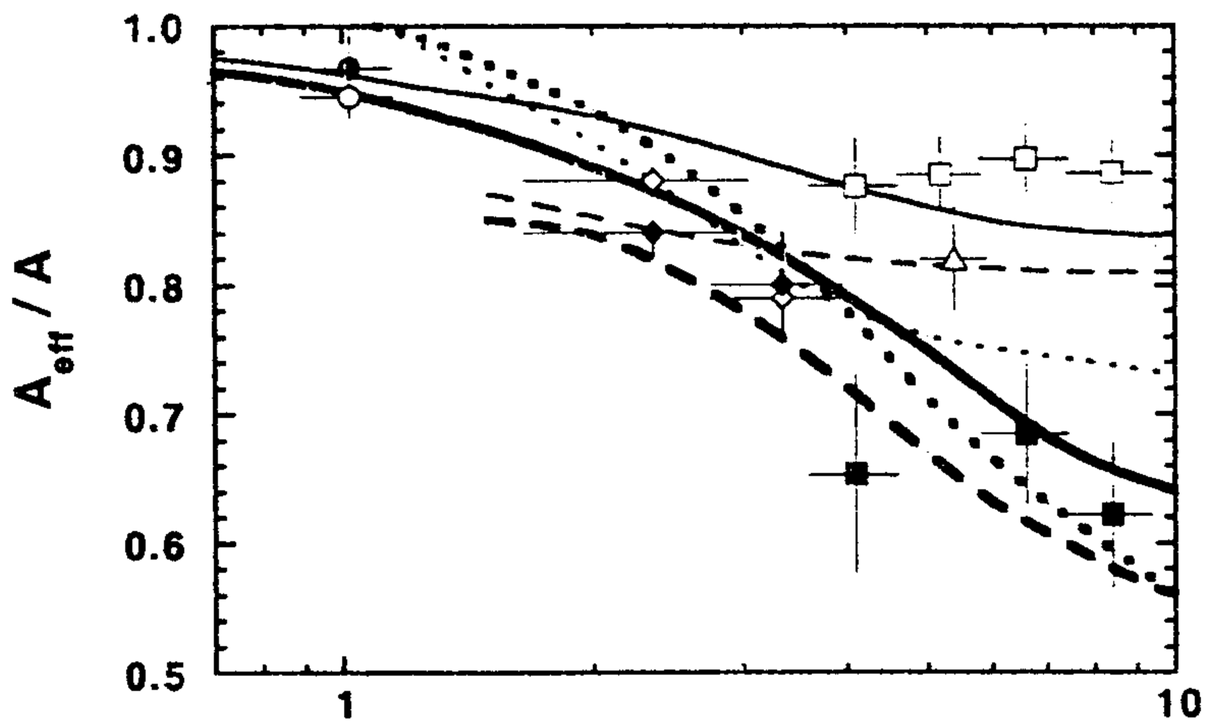

Fig. 16. Shadowing effect measured for C (open symbols) and Pb (close symbols). Our data (circles) and some data available from literature (rhombs)[39] , (triangles)[42] and (squares)[41] are shown. Lines are VMD different predictions (solid lines)[40] , (dashed lines)[21] and (dotted lines)[20]; thin lines are the predictions for C, while thick lines for Pb.

Finally Fig. 16 shows how well the average values of our result on C and Pb in the F_{15} resonance energy region agree with the low energy prediction of a recent shadowing model,[40] while older and simpler shadowing models give very different evaluations of the shadowing threshold region around 1 and 2 GeV, mainly due to different ρ meson cross section parametrization.[20,21] Shadowing effect is quantitatively evaluated by the parameter $A_{eff}/A = \sigma_A/(Z\sigma_p + N\sigma_n)$ which represents the effective number of nucleons seen by the incoming probe. If this parameter is less than one it means that nucleons which are in the center of the nucleus are shadowed by the more external ones.

5.3. *Nuclear density effect*

Nuclear medium effects are generally expected to be a function of nuclear parameters like the average nuclear density $\rho(A)$ or the mass number A. To check this expectation we fitted the total cross section values obtained on different nuclei for each invariant mass W with a linear function of the nuclear density $\sigma_A(W)/A = b(W)[1 + \beta(W)\rho(A)]$.

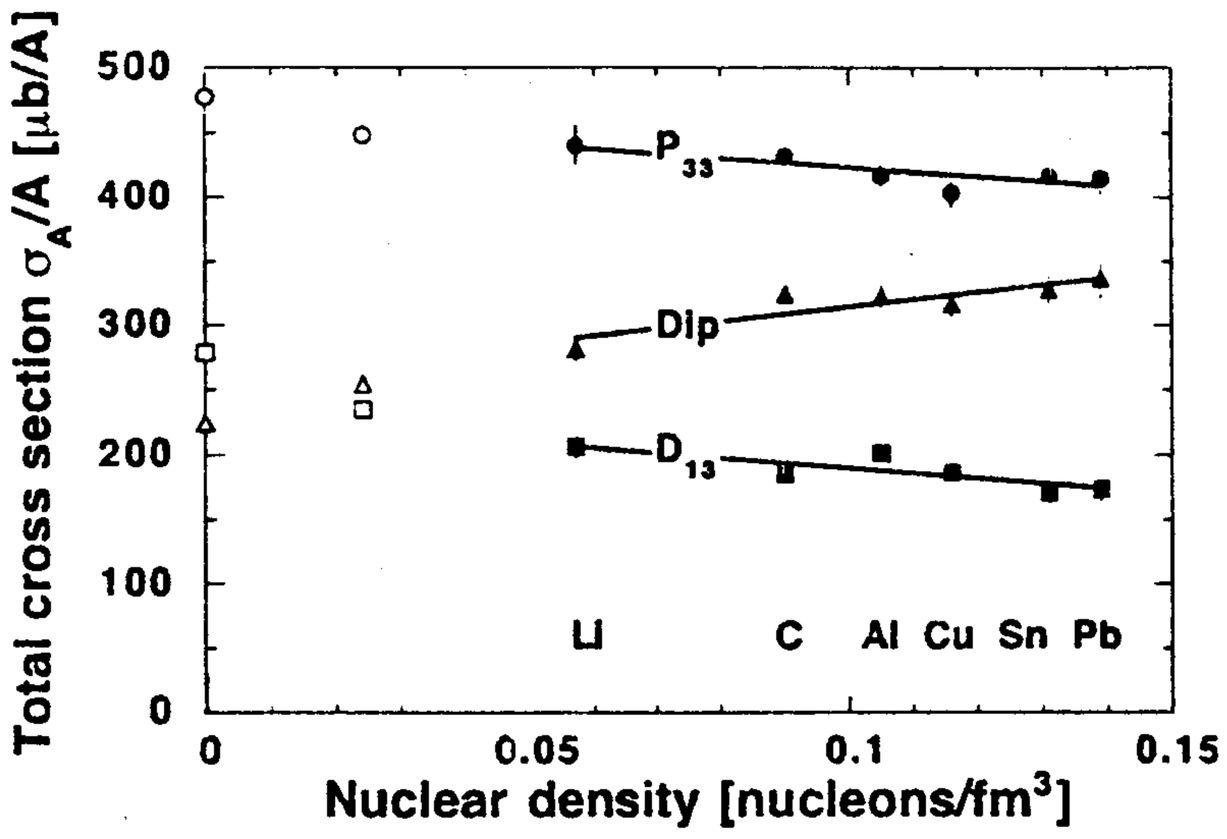

Fig. 17. Total cross section as function of the nuclear density ρ, for three different values of invariant mass corresponding to the P_{33} peak (circles), the D_{13} peak (squares) and the dip region between them (triangles). Our data (close symbols) have been fitted linearly in ρ: $\sigma_A/A = b(W)[1 + \beta(W)\rho(A)]$. Also shown are the Daresbury data for hydrogen (which ρ is arbitrarily assumed equal to 0) and deuterium ($\rho = 0.024$).

Fig. 17 shows three examples of these linear fits to our data for the given values of invariant mass corresponding to the P_{33} resonance, to the D_{13} resonance and to the dip region between them. In the fits we assumed that the average nuclear densities were $\rho(A) = 3A/4\pi R^3$ with $R^2 = 5 < r^2 > /3$, $< r^2 >$ being the rms electron scattering radius of the nucleus.[43] As it is shown, these data are well reproduced by a

linear fit, whose extrapolation at low density is in fairly good agreement with proton and deuteron values.

Moreover, the slopes of these lines are negative for the two resonance peaks while positive for the dip region, in agreement with the observed broadening of the resonances which increases with the density of the nucleus.

In fig. 18 are shown all the linear coefficent $\beta(W)$ values obtained from our data, not including the proton and deuteron points, together with the ones obtained from the data measured at higher energies on the same nuclei,[9] except the lithium. As shown the qualitative energy behavior for $\beta(W)$ parameter is very close to the one obtained for the ratio of cross sections shown in Fig. 15, thus experimentally indicating that nuclear medium effect really increases with the nuclear density, at least up to the D_{13} region. In the F_{15} region, where the non resonant background is large and where many resonances overlap, no definite indication can be derived.

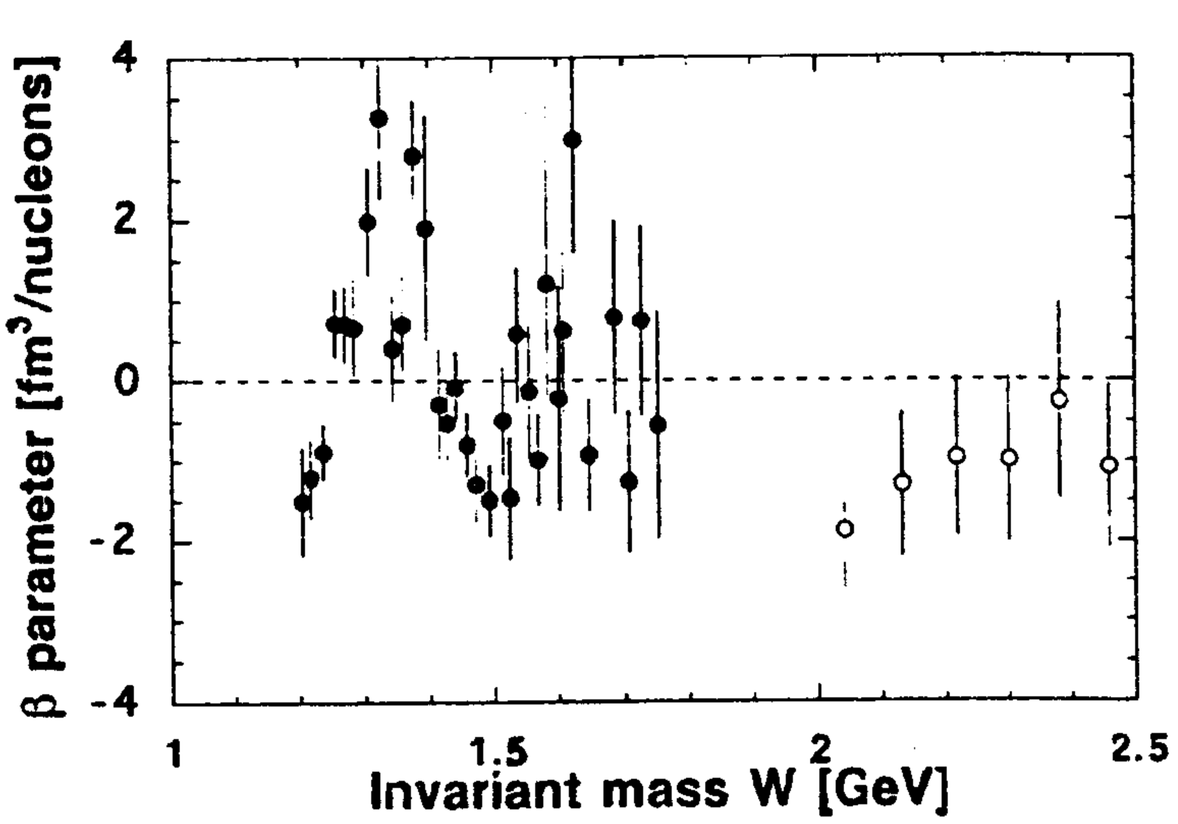

Fig. 18. Linear coefficient β derived for each invariant mass W from our data on Li, C, Al, Cu, Sn and Pb (close circles) and from Daresbury data on C, Al, Cu, Sn and Pb (open circles).

It is worth to mention that we also fitted our data to a power law $\sigma_A(W)/A = a(W)A^{\alpha(W)}$: the result for the energy dependence of $\alpha(W)$ parameter was very similar to the one for $\beta(W)$ parameter but with a worse total reduced χ^2 (1.62 against 1.03 of the density fit).

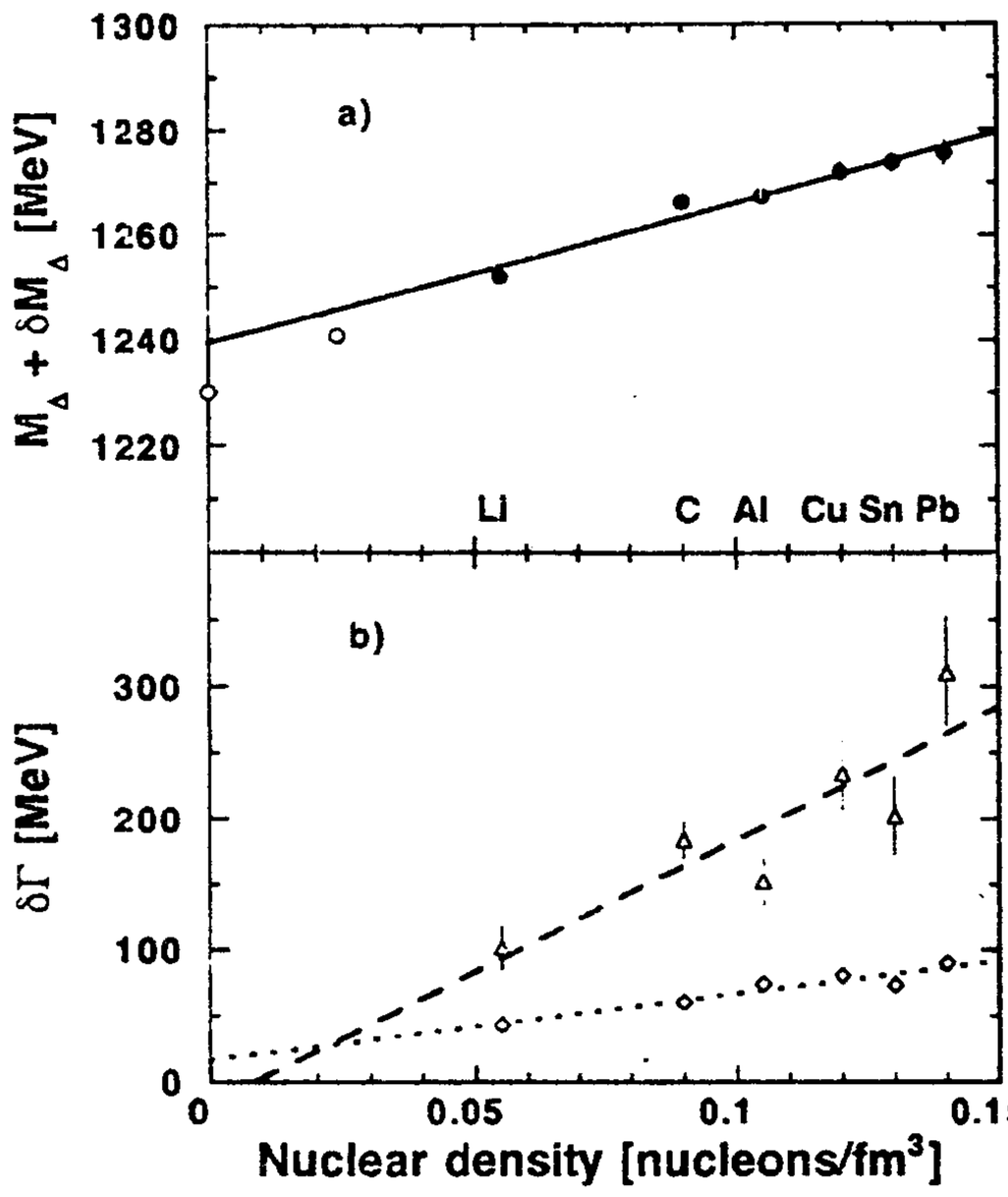

Fig. 19. a) Mass of the Δ resonance extracted from our data on nuclei (close circles) and from hydrogen and deuterium data (open circles); b) broadening due to interaction of the Δ resonance (diamonds) and the average value for N^* resonaces (triangles) extracted from our data. Lines are linear fits in the nuclear density.

For a more quantitative evaluation, the same procedure used to fit the average nucleus cross section data was emploied to fit the data set for the different nuclei, in order to extract δM_Δ, $\delta\Gamma_\Delta$ and $\delta\Gamma_{N^*}$ for each nucleus. The results obtained are plotted in Fig. 19a and 19b versus the nuclear density: as it is seen a nice linear behavior is found in agreement with the prediction of the model (see eqs. 11 and 12).

Therefore it seems reasonable to conclude that due to the resonance propagation and interaction in the photoabsorption process on nuclei the Δ-mass increases with the nuclear density up to few tenths of MeV, the Δ-width up to several tenths of MeV, while the averaged N^*-width up to few hundreds of MeV.

6. CONCLUSION

We have measured the total photoabsorption cross section for several nuclei in the energy range $300 \div 1200$ MeV, using the photohadronic technique with a 4π NaI detector to detect hadronic events and a lead-glass counter to tag the electromagnetic ones. From the comparison between the new results for nuclei and previous data for the free nucleon, we deduced several aspects of nuclear medium effect:

(a) The Δ-resonance mass and width increase almost linearly with the nuclear density. This means that Δ-resonance photo-excitation, like Δ-resonance hadron-excitation, is not an "universal" nuclear behavior.

(b) Nuclear medium effects produce a larger broadening of the peak for higher nucleon resonances. This broadening increases linearly with the nuclear density and can be explained in terms of a strong hadronic interaction in the propagation of the photoproduced resonances.

(c) At present, no realistic information can be extracted for the mass shifts of the higher resonances in nuclei. Being the nuclear medium effect large for the resonance widths, it will be very interesting to look at the possible mass variations for different resonances.

(d) The systematic reduction of the cross section in nuclei above 600 MeV seems to require a reduction of the elementary coupling and this might be considered in terms of a partial damping of higher nucleon resonance excitation and of the onset of the shadowing effect due to the low-mass component in the hadronic spectrum of the photon.

Clearly, a detailed microscopic theoretical treatments of higher nucleon resonances, like those developed for the Δ are urgently needed in order to describe the data in a less phenomenological framework. Also new experimental data are welcome to fill the existing gap between 1.2 and 1.8 GeV and to give a more definitive answer on the threshold and the rising of the shadowing effect.

7. ACKNOWLEDGMENTS

We are pleased to thank our technicians M. Albicocco, A. Orlandi, W. Pesci, A. Rottura and A. Viticchie for their continuous technical assistance and the ADONE staff for efficiency in running the machine. We are grateful to L.A.Kondratyuk for many useful discussions and to G.Piller, W.Ratzka and W.Weise for providing us with the result of their calculation prior to publication. Finally we thank P.Pedroni for providing us with the data collected at Mainz.

References

1. J.Ahrens, Nucl. Phys. **A 446**, 229c, (1985) and reference therein.
2. J.H.Koch, E.J.Moniz and N.Ohtsuka, Ann. of Phys. **154**, 99,(1984).
3. A.S.Carrol et al., Phys. Rev. **C 14**, 635, (1976).
4. E.A.Arakelyan et al., Sov. J. Nucl. Phys. **38**, 589, (1983).
5. A.K.Ananikyan et al., Sov. J. Nucl. Phys. **46** (2), 208, (1987).
6. N.Bianchi et al., Phys. Lett. **B 299**, 219, (1993).
7. M.Anghinolfi et al., Phys. Rev. **C 47**, R922, (1993).
8. N.Bianchi et al., Phys. Lett. **B 309**, 5, (1993).
9. T.A.Armstrong et al., Phys. Rev. **D 5**, 1640, (1972).
10. T.A.Armstrong et al., Nucl. Phys. **B 41**, 445, (1972).
11. Th.Frommhold, F.Steiper, W.Henkel, U.Kneissl, J.Ahrens, R.Beck, J.Peise and M.Schmitz, Phys. Lett. **B 295**, 28, (1992).
12. Th.Frommhold et al., Z. Phys. **A 350**, 249, (1994).
13. N.Bianchi et al., Phys. Lett. **B 325**, 333, (1994).
14. R.Bergere, Proc.2nd Workshop on Perspectives in Nuclear Physics at Int. Energies, Trieste, March 25-29, 1985, p.153, Eds. S. Boffi, C. Ciofi degli Atti and M.M. Giannini, World Scientific,Singapore 1985.
15. R.C.Carrasco and E.Oset, Nucl. Phys. **A 536**, 445, (1992).
16. L.Kondratyuk, M.I.Krivoruchenko, N.Bianchi, E.De Sanctis, V.Muccifora, Nucl. Phys. **A 579**, 453, (1994).
17. W.M.Alberico, G.Gervino and A.Lavagno, Phys. Lett. **B 321**, 177, (1994).
18. M.M.Giannini and E.Santopinto, Phys. Rev. **C 49**, 1258, (1994).
19. S.V.Akulinichev and A.I.L'vov, Mainz Internal Report **MKPH-T-93-1.**
20. S.J.Brodsky and J.Pumplin, Phys. Rev. **182**, 1794, (1969).
21. K.Gottfried and D.R.Yennie, Phys. Rev. **182**, 1595, (1969).
22. P.Distas and G.Shaw, Nucl. Phys. **113**, 246, (1976).
23. G.Shaw, Phys. Rev. **D 47**, R3676, (1993).
24. G.Piller and W.Weise, Phys. Rev. **C 42**, 1834, (1990).
25. W.Weise, Phys. Rev. Lett. **31**, 773, (1973), and Phys. Rep. **13**, 53, (1974).

26. N.Bianchi et al., Nucl. Instrum. Meth., **A 311**, 173, (1992).

27. M.Taiuti et al., Nucl. Instrum. Meth. **A 297**, 354, (1990).

28. V.S.Barashenkov et al., Nucl. Phys., **A 231**, 462 (1974).

29. K.Baba et al., Nucl. Phys. **A 415**, 462, (1984).

30. V.Muccifora et al., Nucl. Instrum. Meth., **A 332**, 288, (1993).

31. M.Mac Cormick et al., Phys. Rev. C, submitted.

32. R.L.Walker et al., Phys. Rev. **182**, 1729, (1969).

33. H. Arenhövel et al., Nucl. Phys. **A 374**, 521c, (1982).

34. Particle Data Group, Phys. Rev. **D 45**, Part 2, (1992).

35. A.Lepretre et al., Nucl. Phys. **A 367**, 23, (1981).

36. J.Ahrens et al., Proc. Intern. Conf. on High energy physics and nuclear structure (Vancouver, 1979), eds. D.F. Measday and A.W. Thomas (North-Holland, Amsterdam, 1980) p.67.

37. J.Arends, J.Eyink, A.Hegerath, K.G.Hilger, B.Mecking, G.Noldeke and H.Rost, Phys. Lett. **B 98**, 423, (1981).

38. P.Carlos, Proc. Intern. School of Intermediate energy nuclear physics (Verona, 1985), eds. R.Bergere, S.Costa and C.Schaerf (World Scientific, Singapore) p. 1.

39. G.R.Brookes et al., Phys. Rev. **D 8**, 2826, (1973).

40. G.Piller, W.Ratzka and W.Weise, private communication.

41. D.O.Caldwell, V.B.Elings, W.P.Hesse, R.J.Morrison, F.V.Murphy and D.E.Yount, Phys. Rev. **D 7**, 1362, (1973).

42. V.Heynen, H.Meyer, B.Naroska and D.Notz, Phys. Lett. **34 B**, 651, (1971).

43. C.W.De Jager, H. De Vries and C. De Vries, At. Data Nucl. Data Tables **14**, 479, (1974).